International Journal of Geosynthetics and Ground Engineering (2020) 6:39
https://doi.org/10.1007/s40891-020-00223-0

STATE OF THE ART/PRACTICE PAPER

Coupled Flow Modelling in Geotechnical and Ground Engineering: An Overview

Ahmed Ibrahim[1] · **Mohamed A. Meguid**[1]

Received: 19 May 2020 / Accepted: 5 August 2020
© Springer Nature Switzerland AG 2020

Abstract
Particulate flows of combined granular media and fluids are relevant to several natural phenomena as well as industrial applications. In geotechnical engineering, the existing modelling approaches mainly adopt a macroscopic-based continuum analysis which does not provide access to important information on the fluid flow interaction with granular media at the particle scale. Alternatively, particulate modelling can be a powerful tool in understanding the complex micro-mechanics of different phenomena such as landslide, debris flow and internal erosion. However, it is challenging to employ the existing particulate flow models on a scale that practically serves the design and risk assessment for earth structures. With rapid advances in computational power, particulate flow modelling can provide valuable insights on both the micro as well as the macro-scale levels. This paper reviews the different approaches of particulate flow modelling from a multidisciplinary perspective with emphasis on geotechnical applications. In addition, this study presents a summary of the available techniques for reducing the computational cost and highlights the outstanding challenges of particulate flow modelling in geotechnical engineering. This work should provide guidance to geotechnical engineers and researches to determine the appropriate modelling tool to approach particulate flow modelling and identify the major challenges associated with each approach.

Keywords Flow modelling · Ground engineering · Multiscale modelling · Two-fluid model · Particulate flow · Computational fluid dynamics · Discrete element analysis

Introduction

The flow of fluids in particulate media and flow of particle–fluid mixtures are interesting problems and relevant to several industries (e.g., pharmaceutical, chemical, civil, and mining). Understanding the mechanics of these phenomena is critical to solving important engineering problems (e.g., debris flow, soil erosion, liquefaction, and landslides) [1]. Aided by rapid advances in computational resources, coupled flow modelling, hereafter referred to as particulate flow, has significantly developed over the past few decades. The existing state-of-the-art models allow for capturing the detailed characteristics of the flow regime such as particle–particle and particle–fluid interactions. Despite the advances in computational power and algorithms, the simulation of industrial and phenomenological scale problems requires more computational resources than those available for most of engineers and researchers. Various particle upscaling techniques have been developed to overcome this obstacle and reduce computational cost [2–4]. However, it is quite challenging to maintain the intricate level of detail from refined simulations upon the upscaling process. Zhu et al. [5, 6] attribute this issue to the absence of a general theory for particulate flow (e.g., accurate description of momentum transfer) that allows for proper upscaling. Such level of detail might be more important to some applications than others and proper use of different modelling tools and upscaling techniques could result in acceptable results. Therefore, it is essential to have a good understanding of the theoretical aspects, modelling tools, and upscaling techniques in particulate flow modelling.

The interest in fluid-granular media interaction is not new to geotechnical engineering. Examples include mechanical analysis of saturated and unsaturated soils, flow through water-retaining earth structures and rain-driven landslides.

✉ Mohamed A. Meguid
mohamed.meguid@mcgill.ca

Ahmed Ibrahim
ahmed.ibrahim5@mail.mcgill.ca

[1] Department of Civil Engineering and Applied Mechanics, McGill University, Montreal, QC H3A 0C3, Canada

Published online: 16 August 2020

Solid–fluid interaction is commonly estimated through macroscale-based constitutive models. These models utilize a simplified form of fluid flow in soils, e.g., Darcy flow, and constitutively link other parameters such as effective stresses and solid skeleton deformation to the flow variables [7–9]. Such an approach can be appropriate when dealing with quasi-static applications where deformations in the solid skeleton can be neglected. However, when hydrodynamic forces are of significance to the analysis, more complex physics are required to fully resolve the interaction between soil and water and establish proper constitutive models. The major drawback with considering continuum-based analysis is that micromechanics of interest such as the development and evolution of piping or cavity evolution in earth embankments remains not fully understood. On the other hand, performing particulate flow modelling by accounting for the micromechanics of both soil particles and fluid flow can provide a deeper understanding and help improve the existing constitutive models used to capture the response of such applications.

It is notable that most of the major developments in particulate flow modelling were developed in the context of chemical engineering, with a special focus on fluidized beds and pneumatic conveying due to their vast applications. These developments were later incorporated in civil and geotechnical engineering to simulate a variety of phenomena such as liquefaction [10, 11], landslides [2, 12], erosion and cavity evolution [13], riverbed erosion and sediment transport [14, 15], scour around pipelines [16], and debris flow [17, 18]. However, the largest portion of the literature on particulate flow is found and seemingly continues to be, in the context of chemical engineering (Fig. 1). In contrast, civil and geotechnical engineering contribution to the subject is relatively limited. One reason for this limitation is the inherent large-scale nature of geotechnical applications such as earth dams and slope stability, which are computationally expensive to model. It could be argued that applications in chemical engineering are more relevant to particulate flow than geotechnical engineering, however, several geotechnical phenomena such as erosion, debris flow, and liquefaction are strongly relevant to particulate flow modelling and still require an in-depth understanding of the underlying dynamics. Indeed, such limited contribution on the side of geotechnical engineering limits the practitioners' accessibility to case studies and models catered to geotechnical engineering, which in turn hinders our understanding of particulate flow in geotechnical-related applications.

Several reviews of particulate flow modelling have been presented with emphasis on specific aspects of the models. For example, theoretical development and applications [5, 6], multiscale frameworks of multi-level constitutive relationships [3, 19], thermal exchange [20], momentum coupling methods [21], reactive particulate flow systems [22], and model development and modelling tools [23]. Despite the rich knowledge provided in these reviews, they are mainly focused on fluidized beds and pneumatic conveyors, while applications in the ground and geotechnical engineering are seldom discussed. Moreover, to our knowledge, a holistic summary of the methodology, available modelling tools, and upscaling methods focused on geotechnical engineering applications does not exist in the literature. In other words, a 'starter pack' for geotechnical engineering practitioners that aids the selection of appropriate modelling methodology, computationally feasible modelling tools, and proper upscaling technique is not yet available.

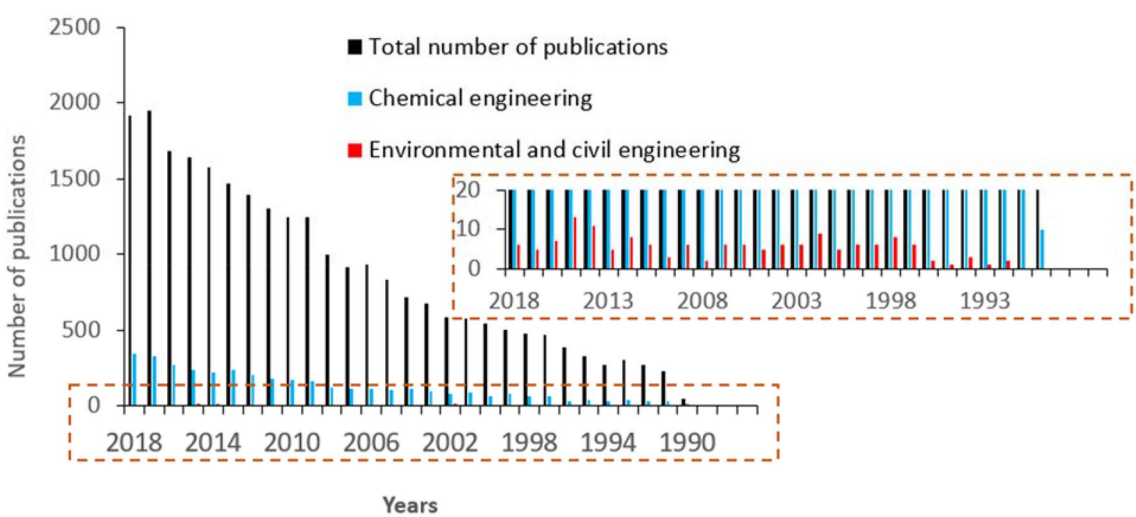

Fig. 1 The total number of publications on the coupling of solid-fluid flow between 1990 and 2018 Source: web of science. Keywords: particulate flow, CFD-DEM, solid-fluid flow coupling

In this work, we aim to present a review of the available approaches for particulate flow modelling with a special focus to geotechnical applications, exploring the advantages and disadvantages of each approach with respect to the scale of the tackled problem. In addition, we review the available modelling tools (open source codes and commercial packages), highlighting the specific features of each package. Finally, we provide a detailed discussion on the current challenges related to multi-scale modelling, upscaling techniques and implementation of boundary conditions. To keep the article size manageable, aspects related to turbulent flow modelling is only briefly discussed for it is considered to be beyond the scope of this work.

The Need for Coupled Flow Modelling in Ground and Geotechnical Engineering

Solid–fluid interaction in geotechnical engineering is a cornerstone in the mechanical analysis and design of earth structures. Existence of water within soils, for instance, fundamentally controls the state of stresses, deformation, and other soil properties. Accounting for such effect is essential for estimating the critical parameters and factors of safety needed for design. The existing conventional methods adopt a macroscopic approach for including such interaction. This macroscopic view considers the properties of the bulk soil masses, either saturated or unsaturated, such as soil weight and shear strength parameters without direct reflection on the particulate nature of soils. Although conventional analysis is viable and can adequately serve the design purposes, it does not allow one to understand important aspects of these systems that can only be understood through the micromechanical analysis of coupled water-soil interaction.

Considering an earth dam for example (Fig. 2), the conventional analysis provides us with insights on the overall stability of the structure or the factors of safety against soil piping and highlights the need for special components such as drains and filters. However, it does not give us sufficient details on the process of internal erosion within the body of the dam where the interaction between soil particles and water needs to be resolved. To track the initiation and propagation of erosion, we need to incorporate coupled (particulate) flow that allows us to access the interparticle and particle–fluid interactions. Another example of the lack of information provided by macroscopic analysis is slope stability, for which rainfall and changes in groundwater levels are major drives. Despite the information we can obtain regarding the potential failure surfaces and factors of safety against failure, particle movement and relocation within the soil pores during water flow remains unknown.

In some situations, conducting particulate flow modelling becomes indispensable, for example, the case of determining the onset of fluidization around leaking pipes. As such leakage can wash soil particles away and can ultimately lead to the formation of cavities and sinkholes, it is important to understand the evolution of such a process at the particle level.

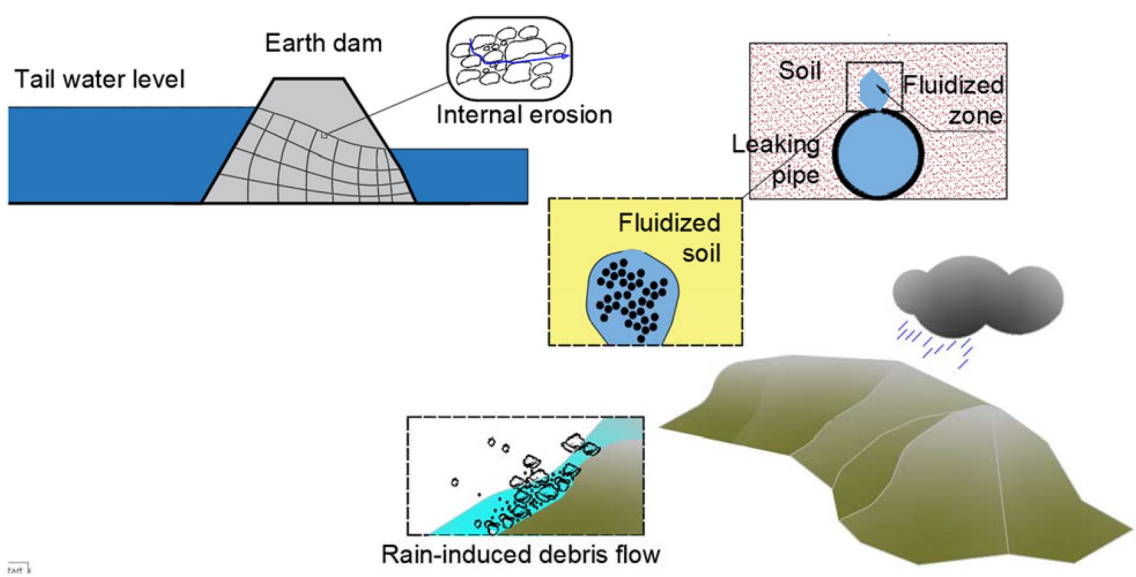

Fig. 2 Examples for coupled water-soil interaction in geotechnical applications; internal erosion in earth dam, soil fluidization and sinkholes due to pipe leakage and rain-induced debris flow

Particle–Fluid Interaction Forces and Momentum Coupling

One of the most challenging aspects of particulate flow modelling is to accurately estimate the interaction forces and momentum transfer between fluid and solid phases. Such estimation depends on the material and flow characteristics of solids and fluids as well as the extent, to which, these interaction forces are considered significant. For instance, in particulate flows with little solid concentration, the solid phase is often dispersed and governed by the hydrodynamic forces with a negligible effect on the fluid motion, i.e., one-way coupling. For denser solid concentration, the motion of the solid particles can affect the fluid streamlines, which is referred to as two-way coupling. In most geotechnical applications, the concentration of solids is typically high and requires four-way coupling, that is, the iterative process of obtaining the mutual impact of solid and fluid phases on each other by accounting for the effect of the changed fluid motion back on particles as well as for particle–particle interactions. In two-way and four-way coupling, it is necessary to ensure that Newton's third law of motion is achieved, i.e., the impact of fluid on solids is equal in magnitude to the impact of solids on the fluid in opposite direction.

Although efforts have been made to resolve fluid-particle interactions, this aspect remains not fully understood and the models we have today are based on empirical or semi-empirical relations. This is because the underlying mechanics of such interaction are very complex and depend on many factors such as particle shape, material properties of solid and fluid phases, and the type of coupling considered in the problem. Nonetheless, the existing models have been proven to be robust and can adequately simulate particulate flow with good accuracy. In this section, we exhibit the existing forces considered in particle–fluid interaction, the theoretical basis and special considerations for each force and the range of application to different flow regimes.

Drag Force

Drag force is a result of fluid shearing on solid particles due to different velocity of each phase and acts in the direction of the relative velocity between fluid and solid particles (Fig. 3) [2]. This force applies to the surface of the solid particle and is often assumed to be effective at the centre of the particle, drag force can be generally expressed as:

$$\boldsymbol{F}_{\mathrm{d}} = \beta\left(\boldsymbol{u}_{\mathrm{f}} - \boldsymbol{u}_{\mathrm{p}}\right), \tag{1}$$

where $\boldsymbol{F}_{\mathrm{d}}$ is the drag force, $\boldsymbol{u}_{\mathrm{f}}$ and $\boldsymbol{u}_{\mathrm{p}}$ are the fluid and solid particle velocities, respectively, and β is the momentum transfer coefficient between fluid and solid particles. One of the early expression for β was presented by Ergun [24]:

$$\beta = \frac{3}{4}\frac{C_{\mathrm{d}} n(1-\alpha)\rho_{\mathrm{f}}}{D}\left|\boldsymbol{u}_{\mathrm{f}} - \boldsymbol{u}_{\mathrm{p}}\right|, \tag{2}$$

where C_{d} is the drag force coefficient, ε is the porosity or fluid volume fraction, D is the diameter of the solid particle, and ρ_{f} is the fluid density. The drag coefficient given by Ergun is:

$$C_{\mathrm{d}} = \frac{200(1-\alpha)}{n\mathrm{Re}_{\mathrm{p}}} + \frac{7}{3\varepsilon}, \tag{3}$$

where Re_{p} is the particle Reynolds number such that: $\mathrm{Re}_{\mathrm{p}} = \rho_{\mathrm{f}} D\left|\boldsymbol{u}_{\mathrm{f}} - \boldsymbol{u}_{\mathrm{p}}\right|/\mu$, and μ is the dynamic viscosity of the fluid. The expression for C_{d} proposed by Ergun is mainly based on the experimental correlations obtained from the fluidization of dense granular beds, thus, it is not considered suitable for more dilute flows ($\varepsilon \leq 0.8$) [25]. Therefore, another expression for C_{d} was proposed by Wen and Yu [26] for flows with $\varepsilon > 0.8$:

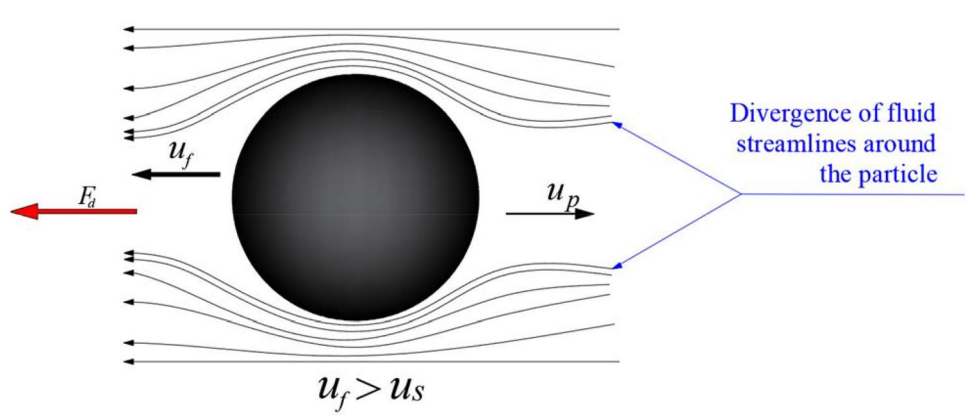

Fig. 3 A schematic illustration of fluid drag force around a solid particle. The directions on the diagram are considered for a case where $u_{\mathrm{f}} > u_{\mathrm{s}}$ (as depicted by the line weight of velocity vectors)

$$C_{\mathrm{d}} = \begin{cases} \frac{24}{\mathrm{Re_p}}\left(1 + 0.15\left(\mathrm{Re_p}\right)^{0.687}\right)\varepsilon^{-2.65} & \mathrm{Re_p} < 1000 \\ 0.44\varepsilon^{-2.65} & \mathrm{Re_p} \geq 1000 \end{cases}. \quad (4)$$

Although combining Ergun's and Wen and Yu's models seems to be sufficient to cover the entire spectrum of porosity that can be encountered, it was found to cause discontinuities in the solution when the porosity fluctuates around 0.8 [27]. Thus, a different correlation for drag force that accounts for porosity correction was introduced by Di Felice [28]:

$$\boldsymbol{F}_{\mathrm{d}} = \frac{1}{2}C_{\mathrm{d}}\rho_{\mathrm{f}}\frac{\pi D^2}{4}\left|\boldsymbol{u}_{\mathrm{f}} - \boldsymbol{u}_{\mathrm{p}}\right|\left(\boldsymbol{u}_{\mathrm{f}} - \boldsymbol{u}_{\mathrm{p}}\right)\varepsilon^{-\chi+1}, \quad (5)$$

where the porosity correction function χ is given as:

$$\chi = 3.7 - 0.65\exp\left[-\frac{\left(1.5 - \log_{10}\mathrm{Re_p}\right)^2}{2}\right]. \quad (6)$$

The estimates for the drag force coefficient found in the literature can be traced back to the correlations of Stokes [29]. Different correlations are proposed by Schiller and Naumann [30], DallaValle [31], and Brown and Lawler [32]. A comparison between these correlations is conducted by Zhao [2]. Zhao concluded that the correlation of Brown and Lawler [32] provides the best match with experimental data, especially for Reynolds number that ranges from 10^2 to 10^4.

Drag force is almost always accounted for in particulate flow modelling. The only exception is dilute flows with a solid concentration of approximately less than 0.1%, in which the effect of particles on the relative velocity of other particles may be neglected and the velocity of the solid particles is nearly the same as the fluid velocity [33]. In geotechnical application, where solid concentration is typically larger than 0.1%, the drag force is always considered.

Pressure Gradient Force

The difference in pressure across a solid particle induces force that acts over the volume of the particle i.e., buoyancy. For a particle with volume (V_{p}) subjected to a pressure gradient (∇p), the resulting force on the particle ($\boldsymbol{F}_{\nabla p}$) is:

$$\boldsymbol{F}_{\nabla p} = -V_{\mathrm{p}}\nabla p. \quad (7)$$

We note that the gradient term in Eq. (7) is the total pressure acting on a particle that contains components of hydrostatic and hydrodynamic pressure. As pointed out by Crowe et al. [34], the hydrostatic pressure component represents the buoyancy effect, thus Eq. (7) can be decomposed as:

$$\boldsymbol{F}_{\nabla p} = \overbrace{-V_{\mathrm{p}}\nabla p_{\mathrm{hydrostatic}}}^{\text{buoyancy force}} - V_p\nabla p_{\mathrm{hydrodynamic}} \quad (8)$$

As can be seen from the equations, the force is proportional to the volume of solid particles and the value of the pressure gradient. In geotechnical applications, this force can be significant, especially the buoyancy component, for submerged solid particles in quasi-static flows.

Other Particle–Fluid Interaction Forces

Other particle–fluid interaction forces can be of significance to particulate flow modelling. These forces include the virtual mass force which accounts for the acceleration of particles within the fluid, Basset force which accounts for the time delay in the boundary layer development, and Saffman and Magnus forces which account for the rotational motion

Table 1 Summary of particle–fluid interaction forces and their significance to geotechnical applications

Force	Expression	References	Significance to geotechnical applications
Drag	$\boldsymbol{F}_{\mathrm{d}} = \beta\left(\boldsymbol{u}_{\mathrm{f}} - \boldsymbol{u}_{\mathrm{p}}\right)$ $\beta = \frac{3}{4}\frac{C_{\mathrm{d}}n(1-\alpha)\rho_{\mathrm{f}}}{D}\left\|\boldsymbol{u}_{\mathrm{f}} - \boldsymbol{u}_{\mathrm{p}}\right\|$ $C_{\mathrm{d}} = \begin{cases} \frac{24}{\mathrm{Re_p}}\left(1 + 0.15\left(\mathrm{Re_p}\right)^{0.687}\right)\alpha^{-2.65} & \mathrm{Re_p} < 1000 \\ 0.44\alpha^{-2.65} & \mathrm{Re_p} \geq 1000 \end{cases}$	Ergun [24] Wen and Yu [26]	Significant
Pressure gradient	$\boldsymbol{F}_{\nabla p} = -V_{\mathrm{p}}\nabla p$	Anderson and Jackson [45]	Significant
Virtual mass	$\boldsymbol{F}_{\mathrm{vm}} = \frac{\rho_{\mathrm{f}}V_{\mathrm{d}}}{2}\left(\frac{\mathrm{d}\boldsymbol{u}_{\mathrm{f}}}{\mathrm{d}t} - \frac{\mathrm{d}\boldsymbol{u}_{\mathrm{s}}}{\mathrm{d}t}\right)$	Auton et al. [140]	Significant for highly unsteady flows
Basset force	$\boldsymbol{F}_{\mathrm{Basset}} = \frac{3}{2}D^2\sqrt{\pi\rho_{\mathrm{f}}\mu_{\mathrm{f}}}\int_0^t \frac{1}{\sqrt{t-t'}}\frac{\mathrm{d}}{\mathrm{d}t}\left(\boldsymbol{u}_{\mathrm{f}} - \boldsymbol{u}_{\mathrm{p}}\right)\mathrm{d}t' + \frac{(\boldsymbol{u}_{\mathrm{f}} - \boldsymbol{u}_{\mathrm{p}})_0}{\sqrt{t}}$	Reeks and Mckee [141]	Insignificant
Saffman force	$\boldsymbol{F}_{\mathrm{saff}} = 1.61\rho_{\mathrm{f}}\mu_{\mathrm{f}}D^2\left\|\boldsymbol{\omega}_{\mathrm{f}}\right\|^{-\frac{1}{2}}\left[\boldsymbol{u}_{\mathrm{f}} - \boldsymbol{u}_{\mathrm{p}}\right] \times \boldsymbol{\omega}_{\mathrm{f}}$	Saffman [142, 143]	Significant for high shear flows
Magnus force	$\boldsymbol{F}_{\mathrm{Mag}} = \frac{\pi}{8}D^2\rho_{\mathrm{f}}\left[\left(\frac{1}{2}\nabla \times \boldsymbol{u}_{\mathrm{f}} - \boldsymbol{\omega}_{\boldsymbol{p}}\right) \times \left(\boldsymbol{u}_{\mathrm{f}} - \boldsymbol{u}_{\mathrm{p}}\right)\right]$	Rubinow and Keller [144]	Insignificant

of solid particles. In Table 1 we include a summary of these forces and their significance in geotechnical applications.

In addition to particle–fluid interaction forces, turbulence effect can be significant to particulate flow modelling. Different closure models are usually adopted depending on the nature of the modelled problem. For example, in seepage-type flows, where fluid velocity is typically small turbulence does not have a tangible effect on the flow. As flow might evolve into a more dynamic state (e.g., debris flow), turbulence closures need to be considered to sufficiently capture the energy transport throughout the system. Examples of turbulence closures in particulate flow modelling include Large Eddy Simulation (LES) [35, 36], k–ε [37–39], and k–ω [40–42].

Approaches for Modelling Particulate Flows

The governing equations of particulate flows are challenging to solve analytically due to the various nonlinearities involved and complex boundary conditions encountered in real problems. Therefore, numerical analysis is conventionally used to solve the set of governing equations. From a numerical point of view, the nonlinear partial differential equations can be solved either using the Eulerian approach or the Lagrangian approach. In the Eulerian approach, the flow variables are viewed as a continuum on a spatially fixed or moving grid and the temporal changes in these variables are tracked locally within each computational cell. In the Lagrangian approach, the trajectory and other flow variables of the fluid or the solid particle are tracked overtime for every single particle. Depending on the numerical treatment of both the fluid and the solid phase, particulate flow modelling can be classified into three main categories: (1) Eulerian–Eulerian, (2) Eulerian–Lagrangian, and (3) Lagrangian–Lagrangian (Fig. 4). In the following section, we provide a thorough review of the different numerical approaches for particulate flow modelling and the underlying models presented under each approach.

Eulerian–Eulerian Approach

The purely Eulerian approach (Eulerian–Eulerian) essentially depends on averaging the flow variables of solid particles and fluids. The most common type of averaging is volume averaging as the computations are often conducted within a computational cell of a finite volume [34]. One of the earliest attempts to average fluid flow with dispersed solids was presented by Van Deemter and Van der Laan [43]. The relationship they presented for fluid momentum is:

$$\left(1-\alpha_{\mathrm{d}}\right)\rho_{\mathrm{f}}\frac{\mathrm{D}\boldsymbol{u}_i}{\mathrm{D}t}=\left(1-\alpha_{\mathrm{d}}\right)\rho_{\mathrm{f}}\boldsymbol{g}_i-\frac{\partial}{\partial x_j}\left(p\delta_{ij}-\boldsymbol{\tau}_{ij}\right)+\boldsymbol{f}_i, \quad (9)$$

where $\boldsymbol{u}_i$ is the velocity of the fluid, α_{d} is the volume fraction of the solid particles, ρ_{f} is the fluid density, $\boldsymbol{g}_i$ is the gravitational acceleration, p is the pressure acting on the fluid, δ_{ij} is the Kronecker delta, $\boldsymbol{\tau}_{ij}$ is the shear stress tensor, and $\boldsymbol{f}_i$ is the force per unit volume acting on the fluid from the solid phase. Two problematic terms in this equation are the fluid velocity, $\boldsymbol{u}_i$, and the force acting on the fluid, $\boldsymbol{f}_i$, because they vary significantly with the volume the fluid is averaged over. Moreover, the use of a single value for fluid velocity is not suitable to represent averaged fluid flow, especially in

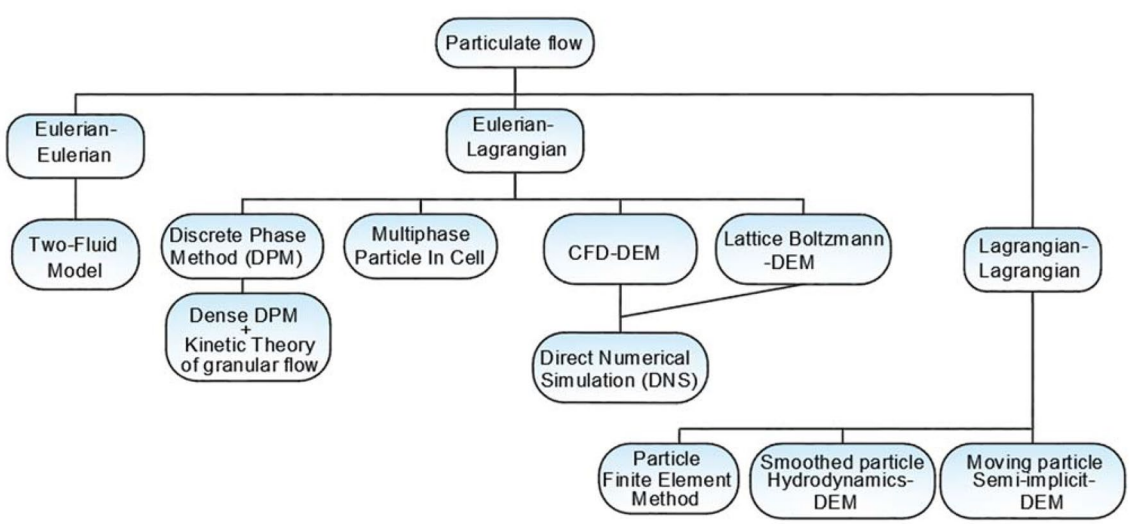

Fig. 4 Different modelling approaches and their corresponding particulate flow methods

turbulent flows. Marble [44] proposed a similar averaging procedure but ignored the effect of the solid phase on the fluid. This equation was derived for particulate flow with dilute dispersed solids. The equation presented by Marble is:

$$\rho_{\mathrm{f}}\frac{\partial \boldsymbol{u}_i}{\partial t}+\rho_{\mathrm{f}}\boldsymbol{u}_j\frac{\partial \boldsymbol{u}_i}{\partial x_j}=-\frac{\partial p}{\partial x_i}+\frac{\partial}{\partial x_j}\boldsymbol{\tau}_{ij}+\boldsymbol{f}_i, \tag{10}$$

where the notation in Eq. (10) denotes the same variables as those in Eq. (9). The term $\boldsymbol{f}_i$ on the right-hand side of Eq. (10), resembles the effect of the fluid motion on the dispersed solid particles. This essentially represents one-way coupling since the effect of the solid particles on the fluid is neglected. This equation is often referred to in the literature as the "dusty gas equation". Anderson and Jackson [45] proposed an averaging technique to transform the point variables (discrete) to a locally averaged values (continuous) over a volume that is large enough to contain many particles, yet, small compared to the dimensions of the system. They presented the following form of the governing equations for mass and momentum conservation:

$$\frac{\partial \varepsilon}{\partial t}+\frac{\partial \varepsilon \boldsymbol{u}_{\mathrm{f}i}}{\partial x_i}=0, \tag{11}$$

$$\frac{\partial (1-\varepsilon)}{\partial t}+\frac{\partial (1-\varepsilon)\boldsymbol{u}_{si}}{\partial x_i}=0, \tag{12}$$

$$\rho_{\mathrm{f}}\varepsilon\left[\frac{\partial \boldsymbol{u}_{\mathrm{f}i}}{\partial t}+\boldsymbol{u}_{\mathrm{f}j}\frac{\partial \boldsymbol{u}_{\mathrm{f}i}}{\partial x_j}\right]=\frac{\partial \boldsymbol{\varepsilon}^{\mathrm{f}}_{ij}}{\partial x_j}+\varepsilon\rho_{\mathrm{f}}\boldsymbol{g}_i-\boldsymbol{f}_i, \tag{13}$$

$$\rho_{\mathrm{s}}(1-\varepsilon)\left[\frac{\partial \boldsymbol{u}_{\mathrm{s}i}}{\partial t}+\boldsymbol{u}_{\mathrm{s}j}\frac{\partial \boldsymbol{u}_{\mathrm{s}i}}{\partial x_j}\right]=\frac{\partial \boldsymbol{\epsilon}^{s}_{ij}}{\partial x_j}+(1-\varepsilon)\rho_{\mathrm{s}}\boldsymbol{g}_i+\boldsymbol{f}_i, \tag{14}$$

where ε is the porosity or volume fraction of the fluid in the averaged volume, $\boldsymbol{u}_{\mathrm{f}i}$ and $\boldsymbol{u}_{si}$ are the local mean velocity of the fluid and solid particles, respectively, ρ_{f} and ρ_{s} are the mass density of fluid and solids, respectively, and $\boldsymbol{f}_i$ is the average force exerted by the solid particles on the fluid estimated over the solid volume fraction. The first term on the right-hand side in Eqs. (13) and (14) lumps the overall stresses acting on the fluid and the solid particles:

$$\boldsymbol{\varepsilon}^{\mathrm{f}}_{ij}=-p^{\mathrm{f}}_i\delta_{ij}+\varepsilon\left(\lambda^{\mathrm{f}}-\frac{2}{3}\mu^{\mathrm{f}}\right)\delta_{ij}\frac{\partial \boldsymbol{u}_{\mathrm{f}i}}{\partial x_i}+\varepsilon\mu^{f}\left(\frac{\partial \boldsymbol{u}_{\mathrm{f}i}}{\partial x_j}+\frac{\partial \boldsymbol{u}_{\mathrm{f}j}}{\partial x_i}\right), \tag{15}$$

$$\boldsymbol{\varepsilon}^{\mathrm{s}}_{ij}=-p^{\mathrm{s}}_i\delta_{ij}+(1-\varepsilon)\left(\lambda^{\mathrm{s}}-\frac{2}{3}\mu^{\mathrm{s}}\right)\delta_{ij}\frac{\partial \boldsymbol{u}_{si}}{\partial x_i}+(1-\varepsilon)\mu^{\mathrm{s}}\left(\frac{\partial \boldsymbol{u}_{si}}{\partial x_j}+\frac{\partial \boldsymbol{u}_{sj}}{\partial x_i}\right), \tag{16}$$

where λ^{f}, μ^{f} and λ^{s}, μ^{s} are the effective bulk and shear viscosities for the fluid and solid phases, respectively, p^{s}_i is the pressure acting on solid particles due to particle contact (interparticle pressure), and p^{f}_i is the local average fluid pressure. As can be seen in Eqs. (15) and (16), several closures are required to obtain the value of solid pressure and the shear stress tensor. These closures also need to be in the form of volume-averaged quantities to be consistent with the set of governing equations.

The Two-Fluid Model (TFM)

The Two-Fluid Model (TFM) emerged as a direct application of the volume averaging techniques. As noted by its name, the solid phase in the flow is treated as a fluid-like continuum with constitutive relationships used to describe the pressure and viscosity terms. In the TFM, both fluid and solid phases are considered as interpenetrating continua in the sense that both phases are expressed as a continuum over

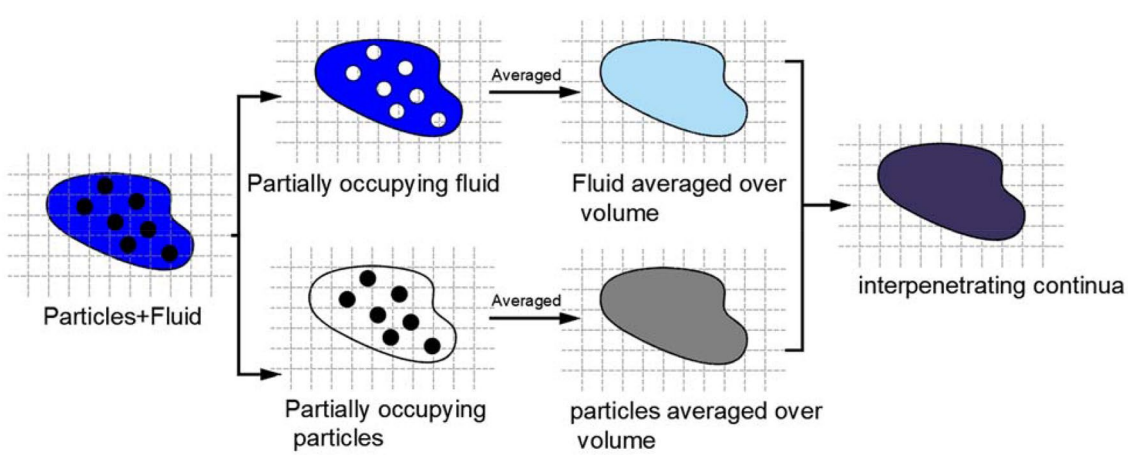

Fig. 5 A schematic illustration of the concept of local averaging and interpenetrating continua

the same averaging volume. The concept of interpenetrating continua may be difficult to visualize because both phases are hypothesized to coexist in the same volume, yet, only partially occupying that volume. In Fig. 5 we try to graphically illustrate this concept.

The core of the TFM is the constitutive relationships for the effective solid pressure p^s, and bulk and shear viscosities, λ^s and μ^s. The early closures for the viscous variables presented by Anderson and Jackson [45], Tsuo and Gidaspow [46], and Kuipers et al. [47] were fully empirical. Despite the simplicity of applying these closures, they did not account for the underlying characteristics of the solid phase rheology [48]. The Kinetic theory of Granular Flow (KTGF) [49–51] is among the most popular methods for pressure and viscosity closures for the TFM. The solid flow variables expressed by KTGF are in terms of the solid volume fraction, $\varepsilon_s = (1 - \varepsilon)$, the normal coefficient of restitution, e, and the granular temperature, θ. For example, the effective shear viscosity of the solid phase (μ^s) is expressed as [52]:

$$\mu^s = \frac{5\sqrt{\pi}}{12}\left(\frac{1}{(1+e)\gamma\left(\varepsilon_s\right)} + \frac{2}{5} + 0.193(1+e)\gamma(\varepsilon_s)\right)\rho_s d\sqrt{\theta}, \tag{17}$$

where, $\gamma(\varepsilon_s)$ is the excess compressibility of an elastic hard-sphere system, and d is the particle diameter. A more detailed discussion on the KTGF is found in Gidaspow [52] and Crowe et al. [34]. Coupling the TFM with KTGF provides the advantage of conducting relatively large-scale simulations. Yet, the constitutive relationships are governed by the microscale characteristics of the flow [48]. This is in contrast to the previously presented empirical constants used for closure, which did not consider the underlying physics of the flow, and perhaps even argued to be unphysical [5, 6].

From the above discussion, it is obvious that the TFM, although being valid for the simulation of some particular problems, lacks the very basic description of particulate dynamics on the microscale. This is because all the interparticle and particle–fluid interactions are indirectly included through averaged values obtained from closures. Crowe et al. [34] argue that the idea of the Two-Fluid Model is essentially flawed because the magnitude of averaging volume might significantly differ from the size of point volume, which does not give accurate representation of the fluctuations in point velocity (Fig. 6). This averaging technique might be valid for gaseous flows where the mixture contains solid components of comparable size to the averaging volume, but cannot be generalized to the broad range of concentrations of dispersed solids in a fluid. For all these reasons, a model is needed to describes the flow characteristics at the particle scale level where no such averaging or heavy reliance on constitutive relationships is used.

Eulerian–Lagrangian Approach

In the Eulerian–Lagrangian approach, the motion of the solid particles is tracked using the Newtonian laws of motion. The tracking of individual particles, with no dependence on a computational mesh, offers the advantage of accounting for the discrete nature of the solid phase. Moreover, the solid–fluid interaction forces (e.g., drag forces and pressure gradient forces) can be directly implemented instead of the previously used indirect averaging approach of the TFM. Indeed, the Lagrangian approach in simulating solid particles does not eliminate the complexity of the estimation of particle fluid-interaction forces because the complexity runs deeper than the issue of volume averaging. However, there is no doubt that the use of the Lagrangian approach for simulating the solid phase has refined the state of simulation and provided access to information on the microscale

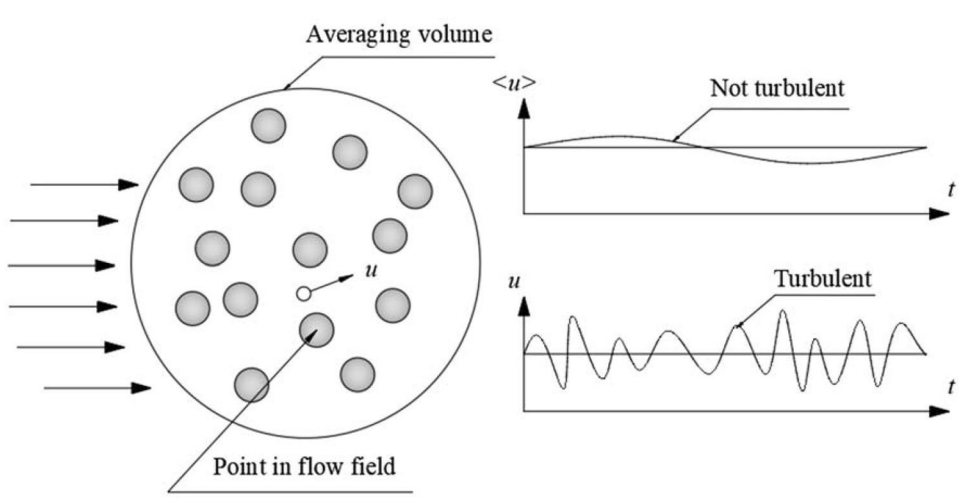

Fig. 6 A comparison of velocity fluctuations between volume-averaged velocity $\langle u \rangle$ and point velocity u

interactions that were impossible to obtain from the Eulerian–Eulerian approach.

Several models have been presented for the simulation of both the Lagrangian and Eulerian numerical treatment in particulate multiphase flows. For the fluid phase (Eulerian), the locally averaged Navier–Stokes equations (Eq. (13)) is the most commonly used. Alternatively, the Lattice Boltzmann method can be used to model the fluid phase, where the fluid flow is modelled via streaming and collision processes on a two-dimensional or three-dimensional lattice. As for the Lagrangian treatment of solid particles, the most commonly used model is the Discrete Element Model (DEM). Other methods such as Discrete Phase Method (DPM) [53–55], Dense Discrete Phase Method (DDPM) [56–58], and Multiphase Particle-In-Cell (MP-PIC) [59–62] have also been used to simulate the motion of solid particles in a Lagrangian framework. In this section, we review the theoretical aspects, coupling strategies and the field of application of the Eulerian–Lagrangian-based models.

Discrete Element Model

The work of Cundall and Strack [63] presented the first model for accurately simulating the motion of granular solids. The translational and rotational motion for a particle i with mass m_i and moment of inertia I_i are described by Newton's second law as:

$$m_i \frac{\mathrm{d}\boldsymbol{v}_i}{\mathrm{d}t} = \sum_j \boldsymbol{F}_{ij}^{\mathrm{c}} + \sum_k \boldsymbol{F}_{ik}^{\mathrm{nc}} + \boldsymbol{F}_i^{\mathrm{f}} + \boldsymbol{F}_i^{\mathrm{g}}, \tag{18}$$

$$I_i \frac{\mathrm{d}\boldsymbol{\omega}_i}{\mathrm{d}t} = \sum_j \boldsymbol{M}_{ij}, \tag{19}$$

where $\boldsymbol{v}_i$ and $\boldsymbol{\omega}_i$ are the translational and angular velocities of particle i, respectively, $\boldsymbol{F}_{ij}^{\mathrm{c}}$ and $\boldsymbol{M}_{ij}$ are the contact force and moment acting on particle i by particle j or wall, $\boldsymbol{F}_{ik}^{\mathrm{nc}}$ is the contactless forces (e.g., electrostatic or liquid bridge forces) acting on particle i by particle k, $\boldsymbol{F}_i^{\mathrm{f}}$ is the particle–fluid interaction force on particle i, and $\boldsymbol{F}_i^{\mathrm{g}}$ is the gravitational force acting on particle i. Figure 7 shows a schematic for the different contact and non-contact forces in a particle i by a particle in contact (j) and a particle not in contact (k).

Cundall and Strack [63] proposed a linear spring-dashpot model to estimate the contact forces, where the spring part of the model is directly related to contact deformation (both normal and tangential); the dashpot part represents the viscous dissipation of the force.

The normal and tangential contact forces in the DEM model can be expressed as:

$$\boldsymbol{F}_{ij}^{\mathrm{cn}} = -K_n \delta_{ij} \boldsymbol{n}_{\mathrm{c}} - C_{\mathrm{n}} \left(\boldsymbol{v}_{\mathrm{c}} \cdot \boldsymbol{n}_{\mathrm{c}} \right) \boldsymbol{n}_{\mathrm{c}} \tag{20}$$

$$\boldsymbol{F}_{ij}^{t} = -K_t \boldsymbol{v}_{\mathbf{c}}^{\mathbf{t}} + C_t \left(\boldsymbol{v}_{\mathbf{c}} \times \boldsymbol{n}_{\boldsymbol{c}} \right) \times \boldsymbol{n}_{\boldsymbol{c}} \tag{21}$$

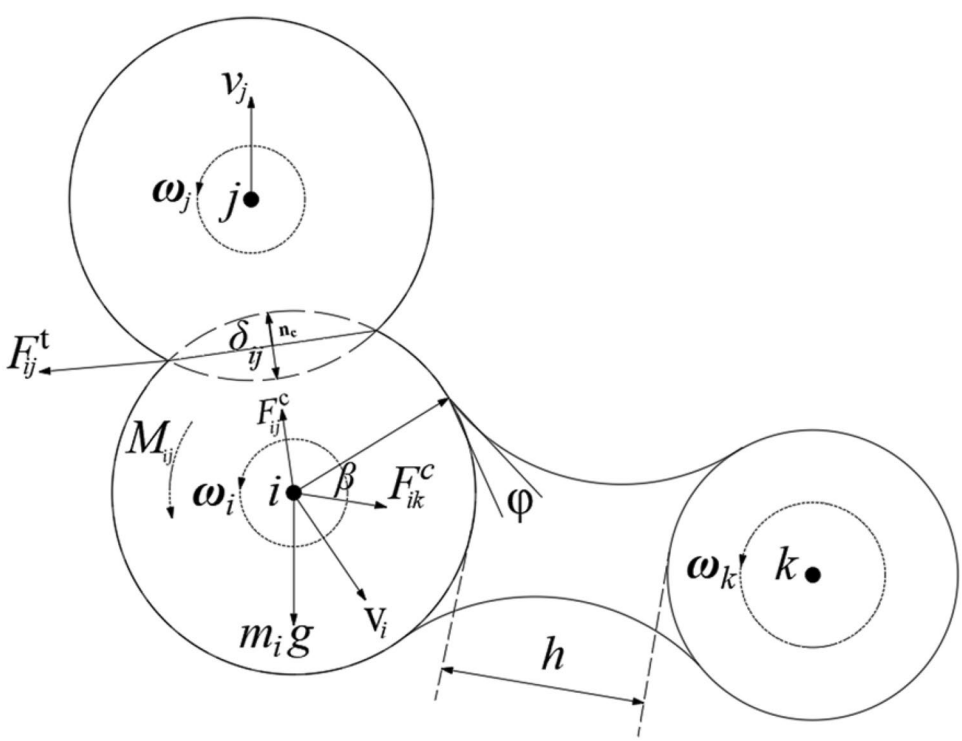

Fig. 7 A schematic for the contact and non-contact forces affecting on particle i by (i) particle j in contact and (ii) particle k that is not in contact

where K_n and K_t are the normal and tangential spring stiffness, respectively, C_n and C_t are the viscous dissipation coefficients related to the dashpot, $\boldsymbol{v}_c$ is the relative velocity between particles in contact and $\boldsymbol{n}_c$ is the normal unit vector at the contact point. In addition to the contact forces between particles, models have been presented to estimate the non-contact forces such as electrostatic forces [64], liquid bridge, and capillary forces [65, 66], and van der Waals forces [67, 68].

CFD-DEM Model

Coupling of DEM and Computational Fluid Dynamics (CFD) has been gaining more popularity since was first introduced by Tsuji et al. [69]. The use of DEM provided unprecedented advantages in simulating the motion of the solid phase of the flow, both translational and rotational, which was not achieved by any of the previous models. In addition, it facilitated the implementation of different particle shapes and interactions. Although nearly all the proposed models, except for Lattice Boltzmann methods, solve volume averaged Navier–Stokes equations, the "CFD" term is exclusively used for the case of solving Navier–Stokes equations with DEM. The two-dimensional soft sphere (i.e., no collision) model presented by Tsuji et al. [69] paved the way for many following developments. Examples for this include the model refinement by Xu and Yu [70] where they presented a detailed coupling technique for the cell-averaged particle–fluid interaction forces. Hoomans et al. [71] introduced a two-dimensional hard-sphere model that accounted for the collision of solid particles based on the conservation of linear and angular momentum of the colliding particles. Shortly after, Kawaguchi et al. [72] successfully extended the model to 3D and obtained good agreement with experimental results.

The aforementioned developments were presented to mainly model solid–gas particulate flows in fluidized beds. However, the robustness and solid theoretical grounds of the approach makes it valid for many other applications. For example, it was extensively used in pneumatic conveying modelling [73–75] and food processing [76, 77]. In geotechnical engineering, the CFD-DEM model was used to model soil liquefaction [10, 11], landslide [2, 12], erosion and cavity evolution [13, 78, 79].

The governing equations for the fluid phase are the same as those in the TFM (Eqs. (11) and (13)) for volume-averaged continuity and Navier–Stokes equations, and the governing equations for the solid phase are the Newtonian equations of motion (Eqs. (18) and (19)). The coupling between CFD and DEM is done as shown in (Fig. 8). Firstly, solid particles are located within each fluid computational cell for porosity/volume fraction calculations. Afterwards, the fluid flow is resolved using the averaged Navier–Stokes equations and the continuity equations to estimate the new fluid position and the fluid forces acting on the solid particles. Following the calculation of the forces on solid particles, the DEM simulation is conducted, typically, with a time step smaller than that required for the CFD simulation to ensure stability. Finally, the updated positions and initial conditions of the solid phase are sent back to the CFD solver to start a new time step until the simulation time is satisfied. This is referred to as "one-way coupling", where only the effect of fluid forces on the solid phase is considered but the effect of the solid phase on the fluid motion is neglected. To conduct two-way coupling, the exported positions and forces from the DEM solver to the CFD solver is used to solve for fluid motion one last time before closing a single time step.

Since the time step required for DEM numerical stability is typically smaller than that used for CFD calculations (e.g., finite volume), the overall speed of simulation is governed by the DEM calculations. To have an insight into this issue, let us consider the DEM time step Δt as [80]:

$$\Delta t \leq \lambda \sqrt{\frac{m}{K_n}}, \tag{22}$$

where λ is a reduction factor to counteract the unphysical energy generation from the numerical approximation in the DEM solution, m is the mass of the particle and K_n is the normal stiffness of the solid particle. On the contrast, the stable time step for the CFD calculations can be determined using the Courant-Fredrich–Lewy (CFL) number [2, 81]:

$$\Delta t \leq \frac{\Delta x}{\varepsilon \left| u_f - u_p \right|}, \tag{23}$$

where Δx is the size of the computational mesh cell for the CFD calculations. From Eqs. (22) and (23), the value of λ is essentially smaller than $1/\varepsilon$. If we consider a typical analysis where the size of the computational cell is fairly larger than the particle size (e.g. 10 times larger), we approximately state that $\Delta x > 10D$, where D is the particle diameter. Where the particle mass is related to the particle diameter by:

$$D = \sqrt[3]{\frac{6m}{\pi \rho_s}}, \tag{24}$$

$$\Delta x > 10 \sqrt[3]{\frac{6m}{\pi \rho_s}}. \tag{25}$$

Now, for the sake of clarification, if we consider sand particles of 1 mm in diameter with a density of 2700 kg/m^3 and normal stiffness of 2×10^5 KN/m, one can tentatively conclude that the stable time step for the DEM is nearly two orders of magnitude higher than that for the CFD. This

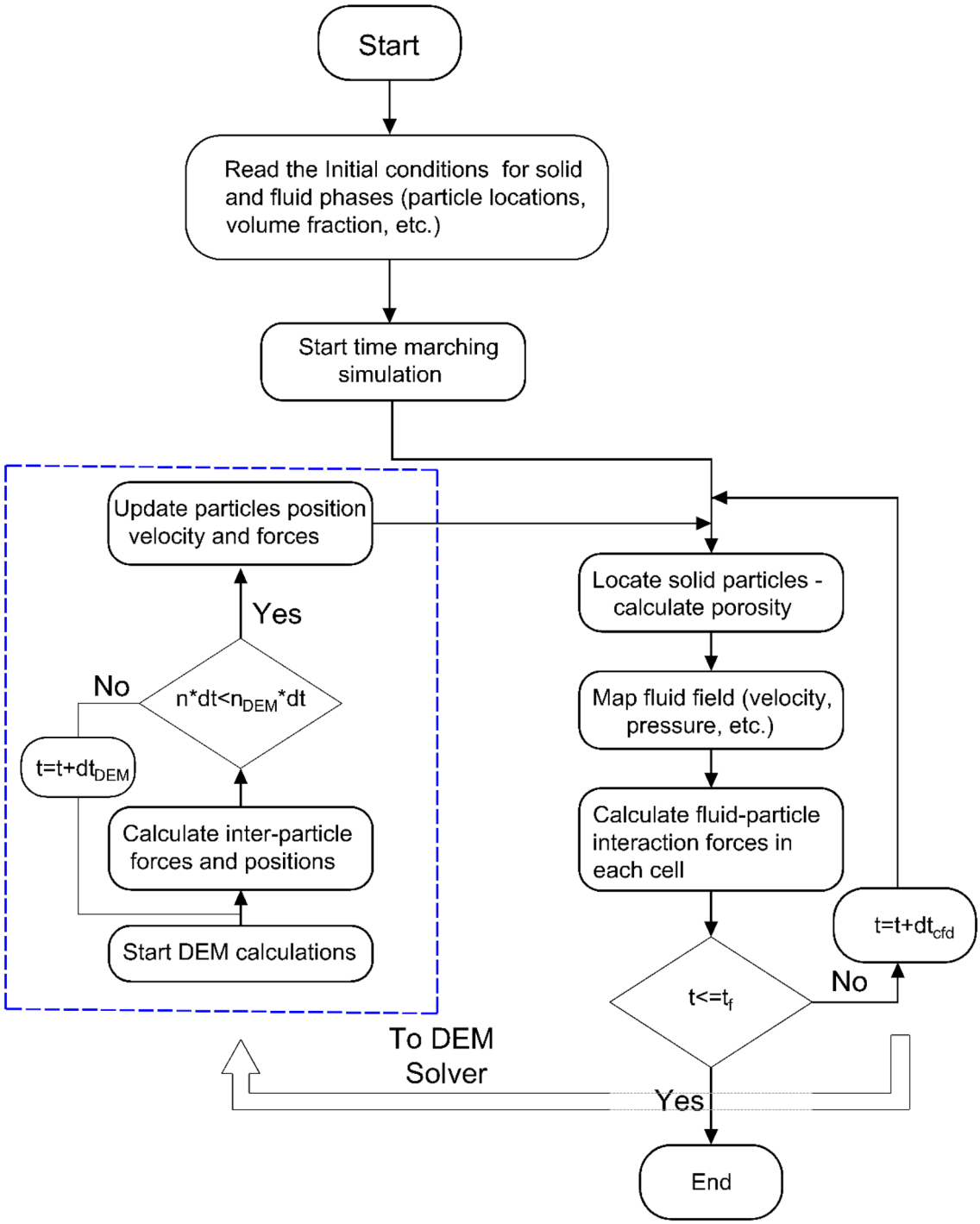

Fig. 8 A flowchart illustrating the solution process of coupled CFD-DEM simulation

conclusion is confirmed by Zhao [2] from a parametric analysis involving DEM time step such that no unphysical kinetic energy is generated in the system on 1250 randomly packed particles with elastic interparticle and wall-particle collision. The stable time step obtained for the DEM computations was found to be two orders of magnitude higher than that of the finite volume scheme used in CFD computations.

One of the drawbacks of the CFD-DEM model is the high computational cost associated with it. Despite its ability to capture the microscale interactions between fluid and solid phases, it takes extensive computational resources to

perform such computations on a large scale. Hence, phenomenological scale simulations using CFD-DEM have not yet been successfully conducted. Reflecting on geotechnical applications, the previously mentioned contributions of the CFD-DEM model in geotechnical engineering have been successfully validated by comparison either to experimental data or known analytical solutions. To get a perspective of this issue, modelling of internal erosion in earth dams might involve billions of DEM particles, the computational capacity needed to simulate is beyond the available resources. Moreover, if such extensive computational resources are available, carrying out such simulations will still not be feasible because it needs to be conductible within resources available for geotechnical engineers.

Another challenge with the application of the CFD-DEM model is the process of assigning and implementing fluid-particle interaction forces. This process can be troubling because both the position and size of the particles can cause disrupted force distribution. For example, as shown in Fig. 9, a particle can exist partially within a cell, which means that duplication will occur if the force is assigned according to the number of the particles in a cell as the particle practically exists in two or more cells [82]. In addition, the ratio between particle size and cell size may cause false estimation of the porosity. As shown in Fig. 9b, if the particle size is large compared to the cell size, porosity can be overestimated. Similarly, it can be underestimated in some of the neighbouring cells. This condition, where particles are smaller in size than computational cells, is often referred to in the literature as "unresolved simulation" [83]. For unresolved simulation, the misplacement of particles can lead to inevitable errors in summing the forces over CFD cells. As this assignment essentially depends on the porosity or the volume fraction of the solid particles, the size of a computational cell should be fairly larger than the size of the largest solid particle such that errors due to porosity fluctuations and force assignment are minimized [82, 84]. A proper ratio between the cell and particle sizes as suggested by Kloss et al. [83] is 10.

It is important to note that the implemented fluid-particle interaction forces such as drag force are estimated for a single particle. Subsequently, for drag force as an example, the effect of surrounding particles on the drag is not considered [5, 6]. Furthermore, to ensure that Newton's third law is not violated (i.e., the forces posed by the fluid on particles and vice versa are equal in magnitude), the forces are computed for each particle in the cell and then summed to obtain the interaction force at the cell scale. The sum of forces estimated for single particles with no account for the effect of other particles will not give an accurate representation for interaction forces. Besides, the previously pointed issues with estimating the volume fraction may give misleading results for the interaction force. The only available way, so far, to overcome these issues is to conduct the calculations using a relatively finer mesh for the fluid and obtain the forces on solid particles by integrating the shear stress over the surface of the particle. This approach eliminates the need for volume averaging and constitutive relationships in the first place and referred to as "resolved" modelling (Fig. 10).

In resolved modelling, the CFD mesh cells are sized to be small compared to interparticle spacing [85]. By considering the solid particles as moving boundaries [86], the fluid-particle interaction forces can be obtained by integrating the shear stresses over the particle's surface [87]. This approach can be practical when simulating relatively large bodies immersed in a fluid. However, for dense particulate systems involving a large number of particles with small interparticle spaces, the resolution of the simulation is most unlikely to be computationally feasible. Thus, the approach is seldom used for practical simulation and is rather used to

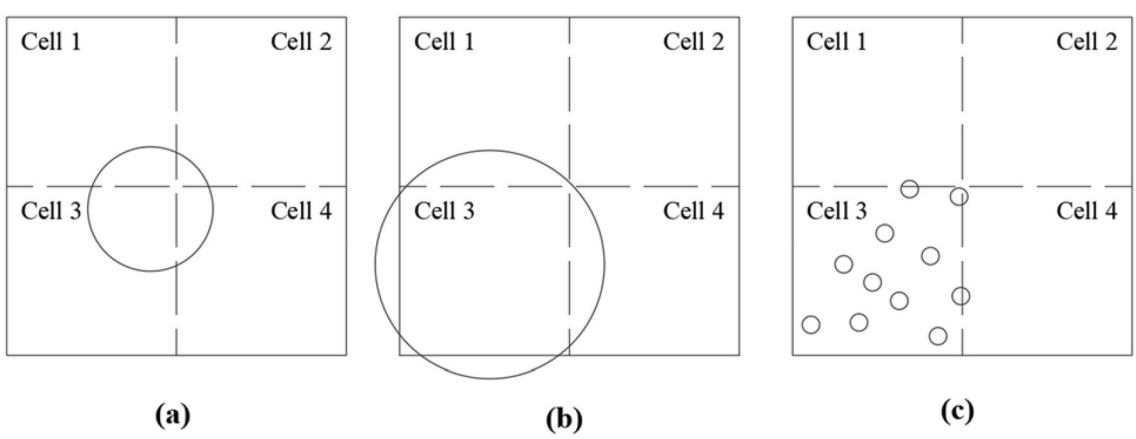

Fig. 9 Different possible configurations of solid particles within a computational cell with respect to particle size and position (adapted from [74])

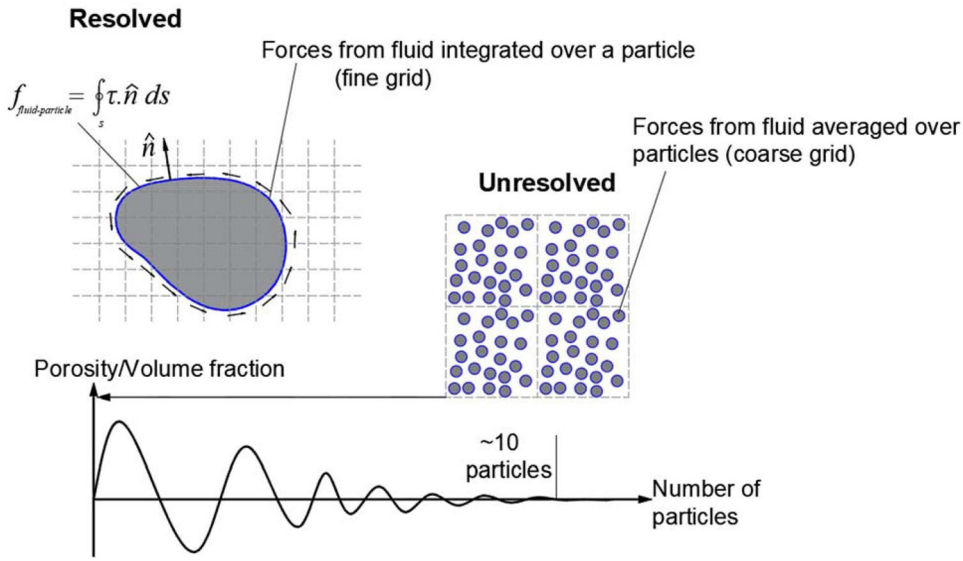

Fig. 10 Illustration for resolved and unresolved numerical simulation for particulate flows and the porosity fluctuations in a control volume with respect to the number of particles

refine the closure models for fluid-particle interaction forces [88]. This can also be seen in the multi-level hierarchy of multiscale simulations [3, 19, 48], where the very basic and most computationally expensive layer of the hierarchy is the direct numerical simulation used to obtain drag closures [19, 89, 90]. In contrast to the case of unresolved modelling, where the overall efficiency of the simulation is dominated by DEM calculations, the efficiency of CFD computations becomes critical in resolved modelling. Thus, it is favourable in this case to use alternative and more efficient methods such as the Lattice Boltzmann Method (LBM) to simulate fluid flow.

Lattice Boltzmann Method (LBM)–DEM

The Lattice Boltzmann Method (LBM) is based on the discretization of the Boltzmann equation in space, time, and velocity field [91]. The early development of the method is known as the Lattice Gas Automata (LGA) [92]. Although this method is originated from the kinetic theory of dilute gases, the continuity and Navier–Stokes equations could be successfully recovered from it up to the second-order in time and space [89, 93]. In the LBM, the fluid is represented by packets of mass with properties characterized by a density distribution function PDF to avoid statistical noises encountered previously in the LGA method. These packets reside at the nodes of a lattice mesh, as shown in Fig. 11, and are allowed to move with prescribed velocity in the specified direction for each node to the neighbouring node (streaming). After the streaming of the packets, the packets/particles colliding at a node change velocity according to certain rules that ensure the conservation of mass, momentum, and energy before and after the collision.

One of the most adopted methods for estimating and redistributing the particle velocities after the collision is the Lattice Bhatnagar–Gross–Krook (BGK) single time relaxation model [93], which is given as:

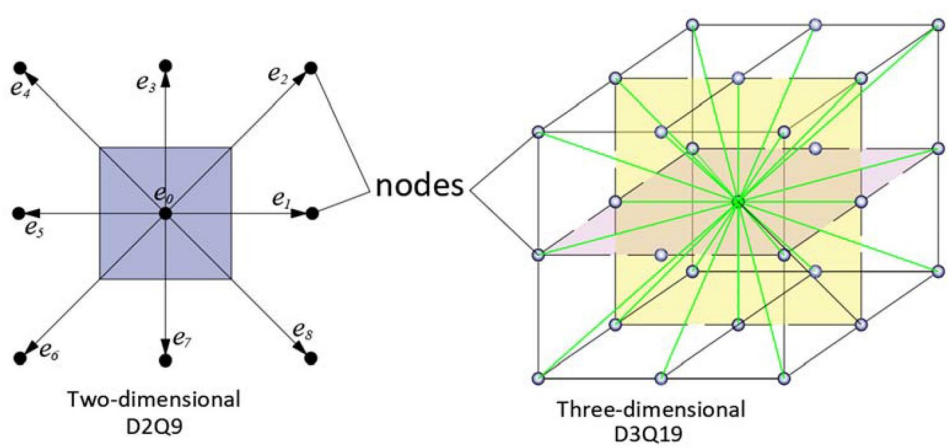

Fig. 11 Two and three-dimensional computational lattice mesh and the principal directions of streaming and collision

$$f_i\left(\boldsymbol{x}+\boldsymbol{e}_i\Delta t, t+\Delta t\right)=f_i(\boldsymbol{x},t)-\frac{\Delta t}{\tau}\left(f_i(\boldsymbol{x},t)-f_i^{\mathrm{eq}}(\boldsymbol{x},t)\right), \quad (26)$$

where $f_i(\boldsymbol{x},t)$ is the probability density distribution of the fluid with velocity $\boldsymbol{e}_i$ located at distance $\boldsymbol{x}$ at time t, τ is the relaxation time, and $f_i^{\mathrm{eq}}(\boldsymbol{x},t)$ is the equilibrium density distribution of the fluid. In Eq. (26), the second term on the right-hand side resembles the collision of fluid packets, and the left-hand side of the equation represents the streaming phase, where the term $(\boldsymbol{e}_i\Delta t)$ is the distance travelled by the particle in the direction of $\boldsymbol{e}_i$. For a two-dimensional simulation, also known as the D2Q9 lattice model, there are eight non-zero velocity distributions at nodes 1–8, and a rest distribution at node 0 (see Fig. 11) [94]. For particulate flows, LBM can be coupled with the DEM by introducing a term for fluid-particle interaction as:

$$f_i\left(\boldsymbol{x}+\boldsymbol{e}_i\Delta t, t+\Delta t\right)=f_i(\boldsymbol{x},t)-\frac{\Delta t}{\tau}(1-B)\left(f_i(\boldsymbol{x},t)-f_i^{\mathrm{eq}}(\boldsymbol{x},t)\right)+B\Omega_i^{\mathrm{s}}, \quad (27)$$

where B is a weighting function to account for the volume fraction of the solid phase (ε) and characterized by the nodal area occupied by the solid particles and the dimensionless relaxation time τ^* as:

$$B(\varepsilon,\tau^*)=\frac{\varepsilon\left(\tau^*-\frac{1}{2}\right)}{(1-\varepsilon)+\left(\tau^*-\frac{1}{2}\right)}, \quad (28)$$

and Ω_i^{s} is known as the "bounce-back term" and is responsible for bouncing back the non-equilibrium part of the distribution, Ω_i^{s} is given as:

$$\Omega_i^{\mathrm{s}}=f_{-i}(\boldsymbol{x},t)-f_i(\boldsymbol{x},t)+f_i^{\mathrm{eq}}\left(\rho,\boldsymbol{v}_{\mathrm{s}}\right)-f_{-i}^{\mathrm{eq}}(\rho,\boldsymbol{v}). \quad (29)$$

A remarkable advantage of the LBM is that it eliminates the need to solve the full Navier–Stokes equations (volume-averaged for particulate flows), instead, it reduces to simpler local operations. This advantage makes LBM easier to program and therefore more efficient in conducting CFD calculations. As pointed by Satofuka and Nishioka [95], the CPU time is reduced to half when LBM is used compared to the conventional CFD methods for the same grid size. However, it is important to keep in mind that in particulate flow simulations involving DEM, the majority of the computational load comes from the DEM part of the simulation. As shown in Fig. 8, several DEM computations are conducted every time step for a single CFD computation because the stable time step of DEM is typically much smaller than this required for CFD [2].

The LBM-DEM has been used successfully applied in various simulations such as fluidized beds [96] sand production [97], internal fluidization and erosion of soil [91], and surface erosion in soils [98, 99]. However, the computational cost of this method for large-scale simulations is still questionable, because, as noted before, the DEM part of the computation remains critical in determining the overall computational cost of the model. This method is more efficient when very fine flow resolution is required as in the direct numerical simulations [48,19d].

Lagrangian–Lagrangian Approach

Throughout the previously discussed models, the fluid flow is always solved locally on a structured or unstructured grid. In contrast, the fully Lagrangian methods adopt trajectory tracking for both fluid and solid phases of particulate flows. One way to conduct such tracking is through a dynamically adaptive grid, where the gird follows the fluid particles/parcels throughout the calculation (e.g., particle finite element method (PFEM)). Alternatively, the fluid can be represented by a set of separate particles with no mesh structure (e.g., smoothed particle hydrodynamics (SPH) [100, 101] and moving particle semi-implicit (MPS) methods [102]). The latter methods are often referred to as meshless/mesh-free or particle methods. Some other methods such as the Material Point Method (MPM) [103, 104] involve the use of a computational grid for intermediate calculations, yet, it is overall considered as a particle method.

Lagrangian tracking provides the advantage of accurately modelling highly convective flows, fragmentation, and free surface flows. This is because the errors associated with the discretization of the convective terms in the Eulerian solvers such as finite volume and finite differences no longer exist. However, particle tracking on a large scale, semi-implicit solutions that require solving Poisson's equation for the pressure field, and dynamic mesh adaptations in the Lagrangian methods may results in higher computational cost as opposed to conventional mesh-based methods such as the Finite Volume Method (FVM). In the following section, we review the theoretical aspects, models, and applicability to geotechnical engineering of some of the major Lagrangian–Lagrangian models in the literature.

Smoothed Particle Hydrodynamics (SPH)

Smoothed particle hydrodynamics (SPH) has been first developed in the field of astrophysics by Lucy [100] and Gingold and Monaghan [101]. Later on, the method was extensively used in hydrodynamic modelling and computational fluid dynamics. In SPH, the fluid continuum is expressed as a set of separate particles that carry information about the flow field such as velocity and pressure. The motion of these particles is governed by conservation laws such as mass, momentum, and energy. The flow properties at one particle are obtained by the super-positioning weighted

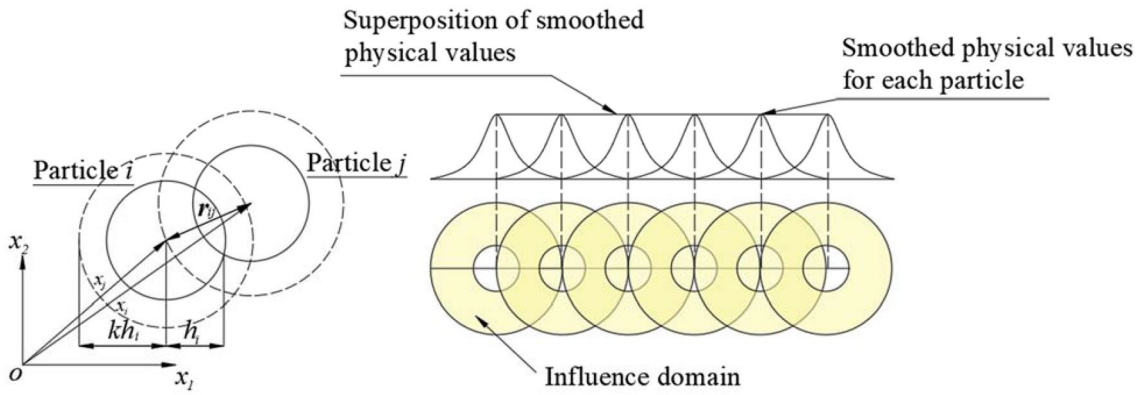

Fig. 12 Illustration of particle representation as moving boundaries and the comparative cell size scale to interparticle spacing

properties of the surrounding particles within a smoothing length, h, via a smoothing function known as the smoothing kernel W (Fig. 12). For instance, at a particle i, the value of a flow variable is the smoothed sum of the variable at a set of particles j that exist within the smoothing length κh, where κ is typically taken as 2 [105].

For a particle i, an averaged property $f(x)_i$ is expressed as:

$$f(x)_i = \sum_{j=1}^{N} m_j \frac{f(x)_j}{\rho_j} W\left(\left|\boldsymbol{r}_j - \boldsymbol{r}_i\right|, h\right), \tag{30}$$

where N is the count of particles that exist within the smoothing length, m_j is the mass of particle j, and $\boldsymbol{r}_i$ and $\boldsymbol{r}_j$ are the position vectors for particles i and j respectively. The gradient of $f(x)_i$ can be estimated by applying Gauss's theorem to the integral of $f(x)_i$ assuming full compact support (i.e., surrounding particles fully exist within a non-truncated sphere of radius κh) as:

$$\nabla f(x)_i = \sum_{j=1}^{N} m_j \frac{f(x)_j}{\rho_j} \nabla W\left(\left|\boldsymbol{r}_j - \boldsymbol{r}_i\right|, h\right). \tag{31}$$

The continuity and Navier–Stokes equation in SPH framework is expressed as:

$$\left(\frac{\mathrm{D}\rho}{\mathrm{d}t}\right)_i = \sum_{j=1}^{N} m_j \left(\boldsymbol{u}_j - \boldsymbol{u}_i\right) \nabla W\left(\left|\boldsymbol{r}_i - \boldsymbol{r}_j\right|, h\right), \tag{32}$$

$$\left(\frac{\mathrm{D}\boldsymbol{u}}{\mathrm{d}t}\right)_i = -\sum_{j=1}^{N} m_j \left(\frac{p_j}{\rho_j^2} + \frac{p_i}{\rho_i^2}\right) \nabla W\left(\left|\boldsymbol{r}_i - \boldsymbol{r}_\mathrm{j}\right|, h\right) + \sum_{j=1}^{N} \boldsymbol{\Pi}_{ij} + \boldsymbol{f}_{\mathrm{b}i}, \tag{33}$$

where $\boldsymbol{\Pi}_{ij}$ is the artificial viscosity term included to ensure the stability of the calculations and $\boldsymbol{f}_{\mathrm{b}i}$ is the body force acting on particle i. $\boldsymbol{\Pi}_{ij}$ is expressed as [106]:

$$\boldsymbol{\Pi}_{ij} = \frac{m_j\left(\mu_i + \mu_j\right)\left(\boldsymbol{r}_i - \boldsymbol{r}_j\right) \cdot \nabla_i W_{ij}}{\rho_i \rho_j \left(\boldsymbol{r}_i - \boldsymbol{r}_j\right)^2} \left(\boldsymbol{u}_i - \boldsymbol{u}_j\right) \tag{34}$$

where $\nabla_i W_{ij}$ is equivalent to $\nabla W\left(\left|\boldsymbol{r}_i - \boldsymbol{r}_\mathrm{j}\right|, h\right)$. More detailed discussion on the derivation and implementation of SPH original formulations can be found in [107].

Over the past few decades, the SPH method has undergone several developments such as the projection-based velocity field decomposition [108], Higher-Order Laplacian formulation for pressure estimation [109], enforcing conservation of angular momentum [110], optimised particle shifting technology [111], higher-order differential operators [112, 113], enhanced hydroelastic coupled solver for fluid–structure interaction (FSI) [114], and SPH with numerical diffusive terms δ-SPH [115]. The method was proven to be superior in accuracy compared to other mesh-based methods for free-surface and highly convective flows (e.g., wave breaking).

SPH–DEM

In particulate flow modelling, working within a fully Lagrangian framework can be more computationally convenient as the previously encountered problems due to the unresolved simulation approach in the CFD-DEM is no longer adopted. Potapov et al. [116] presented one of the earliest models for coupling SPH and DEM. In their model, the fluid–solid coupling was achieved by introducing so-called "artificial SPH particles" that are small enough to occupy the interparticle space. The flow of these particles evolves in the same manner as the rest of SPH particles while at the boundaries of solid particles a no-slip condition is enforced to ensure that artificial particles have the same velocity as the solid particles. The fluid-particle interaction forces are then estimated in a resolved manner, similar to DNS, by summing the exerted fluid forces on solids in a direction opposite to

the flow, which can be expressed as an additional term added to Eq. (33).

Following the work of Potapov et al. [116], Sakai and Maeda [117] developed a three-phase SPH–DEM model to simulate seepage failure under sheet piles considering three-phase flow (air, water, and soil). A multi-layer analysis approach was used, where each phase is modelled separately and then connected phases through constitutive models. The soil phase was assumed to be elastic-perfectly plastic, and combining fluid and solid phases was done using the mixture theory [118]. A different approach was presented by Robinson et al. [119] and Kwon and Cho [120] to conduct a two-way coupling of SPH and DEM using the volume-averaged Navier–Stokes equations using discretized fluid-particle interaction forces in SPH framework. More recently, coupled SPH and DEM was used to simulate solid–fluid flows involving free surface and large deformations [121–124]. In geotechnical and civil engineering applications, SPH–DEM has been used to model internal erosion and seepage flow [125], transport of soil–water mixture and flow through porous media [126] and flow through porous media solely using SPH [127, 128], and soil liquefaction and lateral spread [129]. In addition to coupling with DEM, SPH has also been used along with constitutive models for soils to model dynamic soil behaviour such as embankment failure [105], seepage-induced dike failure [130], and soil liquefaction [131]. The summary in Table 2 includes a comparison between different modelling methods highlighting the numerical approach, computational cost, relevant work and applicability in geotechnical and ground engineering.

Modelling Tools

To carry out particulate flow modelling, the previously governing equations need to be converted to computer code. It is common that researches construct their own in-house codes such that the applications are tailored for a special case of analysis. However, building and debugging codes can be a time-consuming process and more importantly, optimizing the code may require skill sets that are not available for most of the civil engineers. Thus, a good knowledge of the available computational packages, either open-source or commercial, is essential to facilitate the modelling process and save time and effort. There are specific calibres for selecting the proper modelling tool such as the numerical methods deployed in the package, the robustness of the solver, and the computational efficiency of the solver. While commercial packages are often preferred for use in industrial applications because of the robustness of the solver and the existence of a Graphical User Interface (GUI), they allow for a small room for development. On the other hand, open-source software, despite being less convenient in terms of use, allow for development and implementing different physics of choice.

The modelling tools are seldom discussed in the major reviews on particulate flow modelling (e.g., Zhu et al. [5, 6], Deen et al. [19], van der Hoef et al. [48]). However, few summaries for the available modelling tools exist in literature within specific contexts such as pneumatic conveying [23, 132], particulate flow in pipes [133], and code parallelization [134]. Although these reviews are not specifically catered to geotechnical engineering applications, most of the included tools have been successfully used to model geotechnical problems. For example, Guo and Yu [13] used coupled COMSOL multi-physics and PFC3D software to evaluate different simulation methods, Shan and Zhao [17] used LIGGGHTS and OpenFOAM to simulate the impact of granular material flow into a water reservoir, and Zou et al. [79] coupled PFC3D with ANSYS Fluent to simulate the progression of internal erosion in gap-graded soils. In this section, we provide a summary of the available modelling tools for particulate flow modelling. The tools are classified with respect to the numerical framework, as discussed in the previous section. Although the complete features of the

Table 2 Summary of particulate flow models and their numerical treatment and computational cost

Model	Treatment of solid phase	Treatment of fluid phase	References	Applicability in geotechnical engineering	Computational cost
TFM	Eulerian	Eulerian	Anderson and Jackson [45]	Limited applicability	Low
DPM	Lagrangian	Eulerian	Vakhrushev and Wu [55]	Not applicable	Moderate
DDPM +KTGF	Lagrangian	Eulerian	Dickenson and Sansalone [53]	Limited applicability	Moderate
MP-PIC	Lagrangian	Eulerian	Andrews and ORourke [59]	Limited applicability	Moderate
CFD-DEM	Lagrangian	Eulerian	Tsuji et al. [69]	Applicable	High
LBM-DEM	Lagrangian	Eulerian	Cook et al. [89]	Applicable	High
MPM	Lagrangian	Eulerian/constitutive relations	Sulsky and Brackbill [104]	Applicable	Moderate–high
SPH–DEM	Lagrangian	Lagrangian	Potapov et al. [116]	Applicable	High
MPS-DEM	Lagrangian	Lagrangian	Sakai et al. [145]	Applicable	High
PFEM	Lagrangian	Lagrangian	Idelsohn et al. [146]	Applicable	Moderate

computational packages are not reviewed here, the relevant literature in which these packages were used is provided for more information.

In particulate flow modelling, the common practice is to link two computational packages, one for simulating the fluid phase and the other for simulating the solid phase. The reason for this is mainly because modelling tools are well-established for simulating the relevant physics of each phase. This is most effective in Eulerian–Lagrangian methods such as the coupling of CFD packages (e.g., OpenFOAM® and ANSYS Fluent®) with DEM packages (PFC3D™, EDEM™, and LIGGGHTS®). Alternatively, a single computational package can be used for simulating both the fluid and solid phases such as MFiX® software. This is more common in the cases where the fluid phase and the solid phase receive the same numerical treatment (e.g., Eulerian–Eulerian or Lagrangian–Lagrangian). The summary provided in Table 3 includes the available packages with respect to the numerical method, the type of the software, whether open-source or commercial, and the relevant literature to each package. As can be seen from the summary, the CFD-DEM approach has the largest number of available modelling tools compared to the Two-Fluid Eulerian model and SPH Lagrangian model. The reason for this is related to the rapid development taking place in the fields of discrete element modelling and computational fluid dynamics, while development is receding on the side of the Two-Fluid Model and the Lagrangian models are still relatively new to the development compared to the other two methods.

Working Across Scales

Among the obstacles in particulate flow modelling to geotechnical problems is the issue of scale. Some of the models such as the Two-Fluid Model are less computationally expensive. However, the particle–fluid interaction in this sort of simulation is not resolved. Therefore, there is always a compromise between the level of detail that computations can capture and the computational cost. For example, the CFD-DEM modelling provides an accurate description of the interparticle and fluid-particle interactions that can be valuable to understand the mechanics of geotechnical problems like internal erosion and cavity evolution. In literature, it is common that the computational codes are verified using a benchmark problem or well-established experimental results. Nonetheless, following the verification phase, the modelling is often applied to a problem at a laboratory bench scale or smaller. Indeed, in these studies, it is pointed out that the computational capacity does not allow for large scale computations. From the engineering perspective, this kind of simulations does not aid the design of new structures or assess the risk to existing ones.

A few attempts have been carried out to overcome the high computational cost through upscaled models or multi-level modelling framework [2–4]. The upscaling process typically involves using larger elements (e.g., discrete element particles) that are relatable to the original and smaller system through certain relations. This can dramatically help reduce the computational cost of simulating large systems such as embankments since the computational load

Table 3 Summary of computational packages for particulate flow modeling. The packages marked with (OS) refer to open-source packages and those marked with (CO) are the commercial packages

method	Solid phase	Fluid phase	Description	Relevant publications
TFM	MFiX® (OS)		Multiphase (solid–fluid) solver based on the TFM model	Fullmer and Hrenya [147]
	OpenFOAM® (OS) twoPhaseEulerFoam solver		Multiphase (fluid–fluid) solver with the option of KTGF for estimating the stresses in the solid phase	Passalacqua and Fox [148]
CFD-DEM	PFC3D™ (CO)	OpenFOAM® (OS) COMSOL® (CO)	PFC3D code for DEM coupled with OpenFOAM and multi-physics COMSOL for fluid flow	Zhou et al. [133] Guo and Yu [13]
	LIGGGHTS® (OS)	OpenFOAM® (OS)	LIGGGHTS (developed from LAAMPS) for DEM coupled with OpenFOAM	Shan and Zhao [17]
	EDEM (CO)	ANSYS Fluent® (CO)	EDEM software for DEM coupled with OpenFOAM and ANSYS Fluent for fluid flow	Sousani et al. [149]
	MFiX-DEM® (OS)		Multi-phase MFiX code with DEM capability for the particulate solid phase	Bakshi et al. [150]
	DPMFoam		OpenFOAM solver for multiphase Eulerian–Lagrangian flows	Fernandes et al. [151]
	ESyS® (OS) YADE® (OS)	OpenFOAM® (OS) OpenFOAM® (OS)	DEM solver (ESyS and YADE) combined with CFD solver OpenFOAM	Zhao et al. [138] Chen et al. [152]
SPH	LOQUAT (OS)		Open-source software for SPH in geotechnical applications	Peng et al. [153]

is assigned to significantly a smaller number of particles. However, it is important to note that using larger elements, such as large parcels of discrete element particles, comes at the cost of losing access to information pertaining to fine particles in the system. This can be observed in some problems such as landslide, where the front propagation of the landslide is mostly governed by the small particles in the landslide. It is then up to the researcher or engineer to decide whether upscaling the system is feasible in terms of the lost information or not. Therefore, it is important for practitioners and researchers to have a good understanding of the upscaling techniques to facilitate making such a decision. In this section, we review three upscaling techniques (1) multi-level closure system, (2) coarse-grain model (parcelling), and (3) hybrid Eulerian–Lagrangian approach.

Multi-Level Modelling Strategy

Using a multi-level modelling strategy was presented by van der Hoef et al. [3], van der Hoef et al. [48], and Deen et al. [19]. This strategy depends on obtaining closure models from smaller and more accurate models that can later be applied to larger and less computationally expensive models. As can be seen in Fig. 13, the base of the hierarchy is a direct numerical simulation which is the most computationally expensive and accurate method. In fact, this technique is not novel to particulate flow modelling in general. For example, in CFD-DEM or LBM-DEM methods, the fluid-particle interaction forces are not resolved for each particle, rather averaged over the cell volume. Thus, drag closures from experimental or direct numerical simulations are often implemented to account for such forces in the simulations. Reflecting back on multi-scale modelling strategy, the same concept holds valid for larger-scale problems.

This modelling strategy, to our knowledge, has not been applied to any geotechnical engineering applications. This is mainly because the model was proposed for fluidized beds, specifically gas–solid simulations. Nonetheless, this concept is quite common in civil and geotechnical engineering and can be seen in design charts and tables obtained from more intricate and more computationally expensive simulations. Thus, adopting some high-fidelity calculations to obtain closures or constitutive relations for problems at a larger scale may be useful to geotechnical problems. Indeed, to do that, extensive computational resources should be employed. However, conducting such highly expensive simulations can provide a better understanding of the mechanics behind many geotechnical problems and help create more robust constitutive relations.

Coarse-Grained Modelling

In discrete element modelling, it is common to make use of larger grains or parcels of particles to reduce the computational load. Such larger grains are often resembled by clumps of soils or larger elements that not only reduce the computational load but also help make the simulation results more realistic. In particulate flow modelling, however, the use of larger grains becomes more complex as the upscaling or parcelling should conserve the fluid-particle interaction forces in addition to the interparticle forces which is only considered in DEM. The behaviour of lumped particles can vary significantly from the original system of smaller particles due to the different effects of forces on smaller particles. The same scenario is to be expected when performing particulate flow modelling as the fluid forces are expected to mobilize fine particles easily compared to larger ones. This becomes critical when conducting certain simulations such as suffusion because the priority is to capture the motion of fine particles and their fate within larger pores. For more dynamic applications such as debris flow, it might be useful to adopt using larger particles.

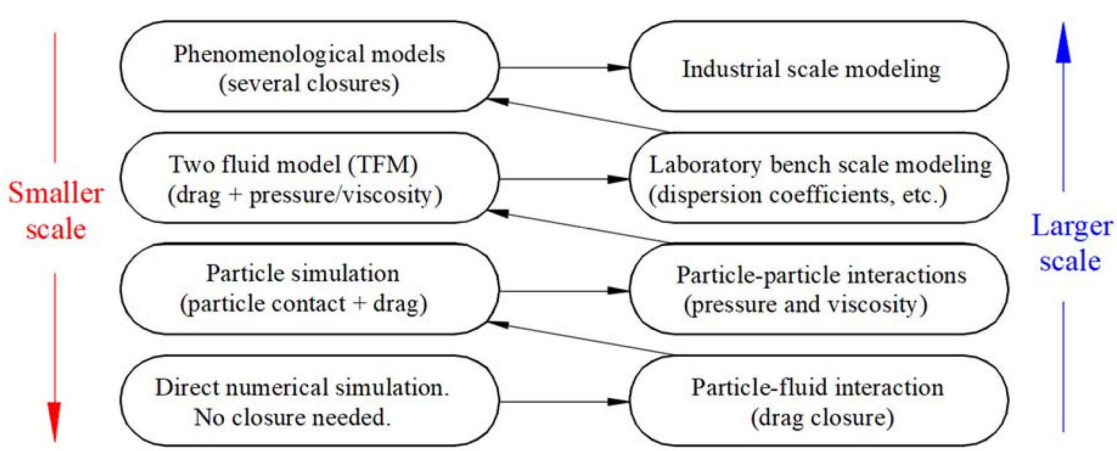

Fig. 13 Multi-scale modelling strategy (after van der Hoef et al. [3])

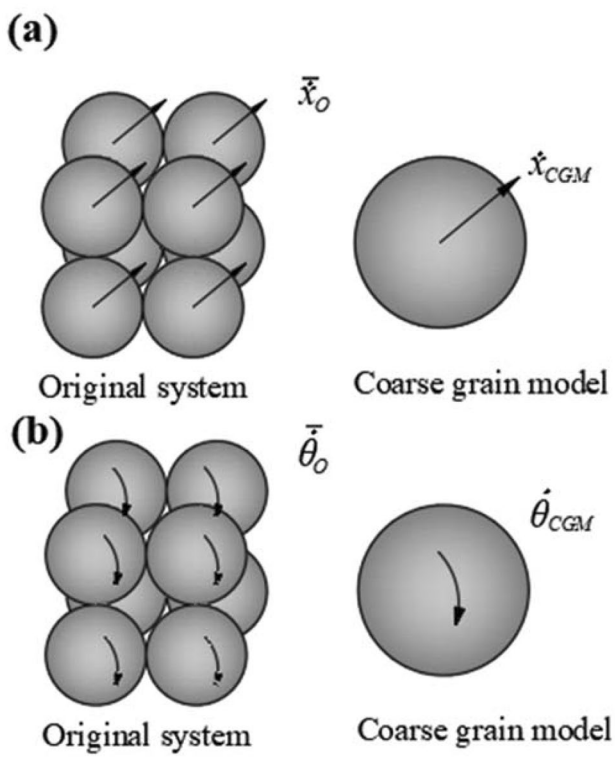

Fig. 14 A schematic of the conservation of **a** translational and **b** rotational motion of the upscaled particles compared to the original set of particles

Sakai and Koshizuka [4] proposed a model for upscaled computations of coupled computational fluid dynamics and discrete element modelling. The criteria behind their model involve preserving the same response of the large (upscaled) particle compared to the original smaller ones to the interparticle forces and fluid-particle interaction forces. As shown in Fig. 14, the model is constructed such that the translational and rotational motion of the large particles are equivalent to those of the original set of smaller particles. The drivers of the motion can be interparticle forces, fluid-particle interaction forces, or any other external forces. For spherical particles, an upscaled particle of radius l larger than the original particles will have a volume that is l^3. Thus, to preserve the same response of translational and rotational motion the two systems are related as [4]:

$$\frac{1}{2}m_{\mathrm{cg}}\dot{\boldsymbol{x}}_{\mathrm{cg}}^2 + \frac{1}{2}I_{cg}\dot{\theta}_{\mathrm{cg}}^2 = l^3\left(\frac{1}{2}m_{\mathrm{o}}\bar{\dot{\boldsymbol{x}}}_{\mathrm{o}}^2 + \frac{1}{2}I_{\mathrm{o}}\bar{\dot{\theta}}_{\mathrm{o}}^2\right), \tag{35}$$

$$\ddot{\theta}_{\mathrm{cg}} = \frac{T_{\mathrm{cg}}}{I_{\mathrm{cg}}} = \frac{\boldsymbol{r}_{\mathrm{cg}} \times F_{\mathrm{cg}}}{I_{\mathrm{cg}}} = \frac{l\boldsymbol{r}_{\mathrm{o}} \times l^3 F_{\mathrm{o}}}{l^5 I_{\mathrm{o}}} = \frac{1}{l}\bar{\ddot{\theta}}_{\mathrm{o}}, \tag{36}$$

where m, $\boldsymbol{x}$, I, θ, and l are the particle mass, position vector, moment of inertia, angular velocity, and the radius ratio between the coarse grain and the small grain, respectively. The subscripts cg and o refer to the coarse grain system and the original system, respectively. In a similar fashion, the relations between the normal and tangential contact forces as well as drag forces are derived based on the volume upscaling ratio l^3.

The results of the coarse grain model were compared to the experimental results of three-dimensional plug flow in a horizontal pipe of Konrad and Davidson [135]. The coarse grain model showed good agreement with the experimental results indicating the model's capability of reproducing the same particle behaviour of smaller particles. However, although that Sakai and Koshizuka [4] point out that the model significantly reduces the computational cost, the speedup of the model was not explicitly stated. It is notable that this model was developed for gas–solid type flows. Nonetheless, it should be applicable to combined liquid–solid flows. From a geotechnical perspective, although particle parcelling for DEM calculations in particulate flows is quite common, this upscaling technique is yet to be applied in geotechnical applications.

Hybrid Eulerian–Lagrangian Models

The pure continuum models, such as the TFM, are by far the most computationally feasible compared to discrete models. The downside of using such models is that they do not provide access to some interstitial information such as the resolved motion of solid particles or the fluid in the vicinity. However, in most cases, such accuracy is only needed locally. This can be seen in many geotechnical applications, for instance, in debris flow the front position and destructive energy are of more interest than other regions, same for piping in earth dams where the detailed flow characteristics around the eroded paths are more important to obtain than other regions. Thus, a smart numerical scheme that combines the accurate discrete element and computational fluid dynamics models along with continuum modelling can help reduce the computational cost of the model and direct the accuracy to certain subdomains of interest.

Hybrid Eulerian–Eulerian and Eulerian–Lagrangian models have been gaining attention recently because of their potential to allocate the computational load to specific subdomains. Such models typically utilize the TFM and DEM-CFD model interchangeably such that the overall execution time of the model is reduced. The model proposed by Hirche et al. [82] is an example of such computations. In this model, the authors introduce so-called pseudo-Lagrangian particles that are included in the overall motion tracking but not in the DEM computations for collision and contact (Fig. 15). Through the use of these particles, the domain can be tuned to use only a portion of the Lagrangian particles for the coupled DEM-CFD calculations while the rest of the pseudo particles are shifted into Eulerian–Eulerian computations.

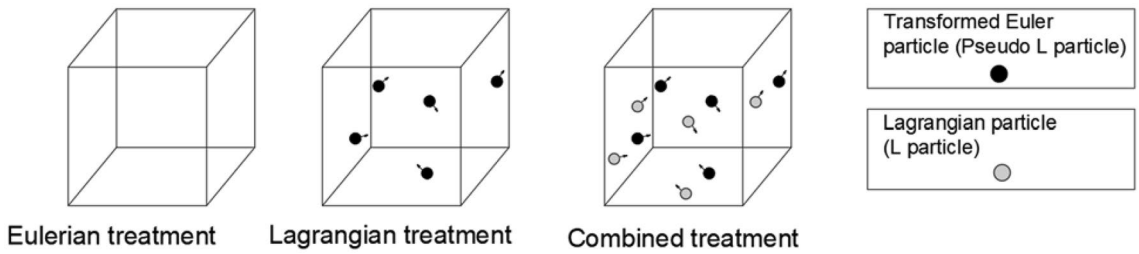

Fig. 15 A schematic showing the computational framework of combined Eulerian–Eulerian and Eulerian–Lagrangian approaches

This model was used to simulate gas–solid flow in fluidized beds and verified by comparison with experimental data from Link et al. [136]. The model speedup could be doubled using a pseudo particle ratio of 50%, compared to sevenfold speedup when using a purely Eulerian approach. Other active attempts are being carried out to develop a robust hybrid model such as the Hybrid MFiX solver [137]. Indeed, performing computations for real-scale systems requires more speedup than what is provided by this model. In addition, the development in hybrid models, to our knowledge, does not allow for a selective allocation of the computational load on a meaningful physical basis. In other words, a smarter model that can locally direct the precession and computational loads is yet to be developed.

Outstanding Challenges of Particulate Flow Modelling in Geotechnical Engineering

Particulate flow modelling can provide valuable data on several geotechnical applications that cannot be obtained through conventional methods or experiments. The main advantage lies in its ability to capture both microscale and macroscale mechanics of the system of the modelled systems. However, as pointed before, the computational cost of performing particulate flow computations on a scale that can serve the design and assessment processes is challenging. In addition to the computational cost, models that can describe complex systems and actual boundary conditions still need to be developed. For example, most of the available literature on particulate modelling in geotechnical engineering use relatively small systems to test the developed models (e.g., Guo and Yu [13], Shan and Zhao [17], Zhao et al. [138], and Cui et al. [91]). These small models often contain a small number of particles that can be handled with the available computational resources; moreover, simple boundary conditions. The two most common boundary conditions are periodic boundary conditions and wall boundary conditions. In real-life applications, systems might have boundary conditions of loading, unloading, water draining, phase change, etc. This complexity is not often encountered in chemical engineering applications such as fluidized bed, for which most of the particulate flow models were developed. Thus, the geotechnical community needs to carry out its own development to tailor models that resemble tackled problems more accurately.

Another outstanding challenge is to develop a multi-resolution framework for particulate flow modelling, such that different spatial resolutions can be included without compromising the accuracy of the simulation. The previously presented hybrid Eulerian–Eulerian Eulerian–Lagrangian approach comes close to achieve this goal through tuning the pseudo Lagrangian particles. However, during the simulation process the resolution can only be globally set for the entire domain rather than incorporating multi-resolution for subdomains. In a recent study, Khayyer et al. [139] proposed an adaptive multi-resolution MPS-based framework to simulate Fluid Structure Interaction (FSI) for elastic structures. The advantage of incorporating different spatial resolutions was found to help enhancing the efficiency of simulation while maintaining the intricacy of high-resolution simulations, as needed. As for particulate flow applications in geotechnical engineering, including robust multi-scale resolution can help enhance the simulation process for many systems that do not require refined spatial resolution for the entire domain, yet gives the advantage of accessing the information related to the micromechanics of the system. This can be particularly useful for modelling localized phenomena such as internal erosion.

More challenges involve dynamic processes related to soils and rocks. In contrast to other applications such as pneumatic conveying and spouted beds where solid particles are mainly mono-sized, soil particle sizes in natural soils can vary significantly, even in a small sample. Along with variable particle size distribution, the cohesion between particles, cementing, and fragmentation of a single soil clump can further complicate the dynamics of particulate flow to a great extent. To tackle these issues, constitutive models that account for water existence, whether static or dynamic, need to be developed.

Summary and Conclusions

In this work, a comprehensive summary of the development and key challenges of particulate flow modelling were presented. The applicability and relevance of the existing particulate flow models to geotechnical applications were discussed. The key issues and challenges identified are:

- Particulate flow modelling, despite its complexity, is needed to gain a better understanding of several geotechnical problems such as failure mechanics of earth structures subjected to high hydrodynamic forces and debris flow.
- In the geotechnical field, such modelling is still underdeveloped and the existing literature mainly addresses small and elementary systems rather than actual structures (e.g., earth dams)
- The high computational cost of conducting coupled solid–fluid modelling and the complexity of boundary conditions in real-life applications are the major obstacles to develop computationally feasible large scale models and to develop constitutive models.
- Robust upscaling techniques and multidisciplinary approaches are needed for closing the gap in this area of research and developing models directed for geotechnical engineers and researchers.

References

1. Wachs A (2019) Particle-scale computational approaches to model dry and saturated granular flows of non-Brownian, non-cohesive, and non-spherical rigid bodies. Acta Mech 230(6):1919–1980. https://doi.org/10.1007/s00707-019-02389-9
2. Zhao T (2017) Coupled DEM-CFD analyses of landslide-induced debris flows, 1st edn. Science Press, Beijing
3. van der Hoef MA, Ye M, van Sint Annaland M, Andrews AT, Sundaresan S, Kuipers JAM (2006) Multiscale modeling of gas-fluidized beds. In: Computational fluid dynamics. advances in chemical engineering, pp 65–149. https://doi.org/10.1016/s0065-2377(06)31002-2
4. Sakai M, Koshizuka S (2009) Large-scale discrete element modeling in pneumatic conveying. Chem Eng Sci 64(3):533–539. https://doi.org/10.1016/j.ces.2008.10.003
5. Zhu HP, Zhou ZY, Yang RY, Yu AB (2007) Discrete particle simulation of particulate systems: theoretical developments. Chem Eng Sci 62(13):3378–3396. https://doi.org/10.1016/j.ces.2006.12.089
6. Zhu HP, Zhou ZY, Yang RY, Yu AB (2008) Discrete particle simulation of particulate systems: a review of major applications and findings. Chem Eng Sci 63(23):5728–5770. https://doi.org/10.1016/j.ces.2008.08.006
7. Yang J, Yin Z-Y, Laouafa F, Hicher P-Y (2020) Hydromechanical modeling of granular soils considering internal erosion. Can Geotech J 57(2):157–172. https://doi.org/10.1139/cgj-2018-0653
8. Schaufler A, Becker C, Steeb H (2013) Infiltration processes in cohesionless soils. Zamm-Z Angew Math Me 93(2–3):138–146. https://doi.org/10.1002/zamm.201200047
9. Vardoulakis I, Stavropoulou M, Papanastasiou P (1996) Hydromechanical aspects of the sand production problem. Transp Porous Med 22(2):225–244. https://doi.org/10.1007/Bf01143517
10. Shamy UE, Zeghal M (2005) Coupled continuum-discrete model for saturated granular soils. J Eng Mech 131(4):413–426. https://doi.org/10.1061/ASCE0733-93992005131:4413
11. Zeghal M, El Shamy U (2004) A continuum-discrete hydromechanical analysis of granular deposit liquefaction. Int J Numer Anal Meth Geomech 28(14):1361–1383. https://doi.org/10.1002/nag.390
12. Shi Z-M, Zheng H-C, Yu S-B, Peng M, Jiang T (2018) Application of CFD-DEM to investigate seepage characteristics of landslide dam materials. Comput Geotech 101:23–33. https://doi.org/10.1016/j.compgeo.2018.04.020
13. Guo Y, Yu X (2017) Comparison of the implementation of three common types of coupled CFD-DEM model for simulating soil surface erosion. Int J Multiph Flow 91:89–100. https://doi.org/10.1016/j.ijmultiphaseflow.2017.01.006
14. Harada E, Ikari H, Shimizu Y, Khayyer A, Gotoh H (2018) Numerical investigation of the morphological dynamics of a step-and-pool riverbed using DEM-MPS. J Hydraul Eng. https://doi.org/10.1061/(Asce)Hy.1943-7900.0001392
15. Harada E, Gotoh H, Ikari H, Khayyer A (2019) Numerical simulation for sediment transport using MPS-DEM coupling model. Adv Water Resour 129:354–364. https://doi.org/10.1016/j.advwatres.2017.08.007
16. Hu D, Tang W, Sun L, Li F, Ji X, Duan Z (2019) Numerical simulation of local scour around two pipelines in tandem using CFD–DEM method. Appl Ocean Res. https://doi.org/10.1016/j.apor.2019.101968
17. Shan T, Zhao J (2014) A coupled CFD-DEM analysis of granular flow impacting on a water reservoir. Acta Mech 225(8):2449–2470. https://doi.org/10.1007/s00707-014-1119-z
18. Jing L, Kwok CY, Leung YF, Sobral YD (2016) Extended CFD-DEM for free-surface flow with multi-size granules. Int J Numer Anal Meth Geomech 40(1):62–79. https://doi.org/10.1002/nag.2387
19. Deen NG, Van Sint Annaland M, Van der Hoef MA, Kuipers JAM (2007) Review of discrete particle modeling of fluidized beds. Chem Eng Sci 62(1–2):28–44. https://doi.org/10.1016/j.ces.2006.08.014
20. Peters B, Baniasadi M, Baniasadi M, Besseron X, Donoso AE, Mohseni M, Pozzetti G (2019) XDEM multi-physics and multi-scale simulation technology: review of DEM–CFD coupling, methodology and engineering applications. Particuology 44:176–193. https://doi.org/10.1016/j.partic.2018.04.005
21. Zhou ZY, Kuang SB, Chu KW, Yu AB (2010) Discrete particle simulation of particle–fluid flow: model formulations and their applicability. J Fluid Mech 661:482–510. https://doi.org/10.1017/s002211201000306x
22. Zhong W, Yu A, Zhou G, Xie J, Zhang H (2016) CFD simulation of dense particulate reaction system: approaches, recent advances and applications. Chem Eng Sci 140:16–43. https://doi.org/10.1016/j.ces.2015.09.035
23. Ariyaratne WKH, Manjula EVPJ, Ratnayake C, Melaaen MC (2018) CFD approaches for modeling gas-solids multiphase flows—a review. Paper presented at the proceedings of the 9th EUROSIM congress on modelling and simulation, EUROSIM 2016, the 57th SIMS conference on simulation and modelling SIMS 2016
24. Ergun S (1952) Fluid flow through packed columns. Chem Eng Prog 48(2):89–94

25. Jackson R (2000) The dynamics of fluidized particles. Cambridge monographs on mechanics. Cambridge University Press, Cambridge
26. Wen CY, Yu YH (1966) Mechanics of fluidization. Chem Eng Progress Symp Ser 62(62):100–111
27. Kafui KD, Thornton C, Adams MJ (2002) Discrete particle-continuum fluid modelling of gas-solid fluidised beds. Chem Eng Sci 57(13):2395–2410. https://doi.org/10.1016/s0009-2509(02)00140-9
28. Di Felice R (1994) The voidage function for fluid particle interaction systems. Int J Multiph Flow 20(1):153–159. https://doi.org/10.1016/0301-9322(94)90011-6
29. Stokes GG (1901) Mathematical and physical papers. Cambridge University Press, Cambridge, p 416
30. Schiller L, Naumann A (1935) A drag coefficient correlation. Z Ver Dtsch Ing 77:318–320
31. DallaValle JM (1948) Micromeritics: the technology of fine particles, 2nd edn. Pitman Pub. Corp, Toronto
32. Brown PP, Lawler DF (2003) Sphere drag and settling velocity revisited. J Environ Eng-Asce 129(3):222–231. https://doi.org/10.1061/(Asce)0733-9372(2003)129:3(222)
33. Elghobashi S (1994) On predicting particle-laden turbulent flows. Appl Sci Res 52(4):309–329. https://doi.org/10.1007/Bf00936835
34. Crowe CT, Schwarzkopf JD, Sommerfeld M, Tsuji Y (2012) Multiphase flow with droplets and particles, 2nd edn. CRC, Oxford
35. Cheng Z, Hsu T-J, Chauchat J (2018) An Eulerian two-phase model for steady sheet flow using large-eddy simulation methodology. Adv Water Resour 111:205–223. https://doi.org/10.1016/j.advwatres.2017.11.016
36. Harada E, Gotoh H, Tsuruta N (2015) Vertical sorting process under oscillatory sheet flow condition by resolved discrete particle model. J Hydraul Res 53(3):332–350. https://doi.org/10.1080/00221686.2014.994139
37. Chauchat J, Guillou S (2008) On turbulence closures for two-phase sediment-laden flow models. J Geophys Res. https://doi.org/10.1029/2007jc004708
38. Ti-J Hsu, Jenkins JT, Liu PL-F (2003) On two-phase sediment transport: sheet flow of massive particles. J Geophys Res 108(14):2223–2250. https://doi.org/10.1029/2007JC004708
39. Bakhtyar R, Yeganeh-Bakhtiary A, Barry DA, Ghaheri A (2009) Two-phase hydrodynamic and sediment transport modeling of wave-generated sheet flow. Adv Water Resour 32(8):1267–1283. https://doi.org/10.1016/j.advwatres.2009.05.002
40. Amoudry LO (2014) Extension of ω turbulence closure to two-phase sediment transport modelling: application to oscillatory sheet flows. Adv Water Resour 72:110–121. https://doi.org/10.1016/j.advwatres.2014.07.006
41. Jha SK, Bombardelli FA (2010) Toward two-phase flow modeling of nondilute sediment transport in open channels. J Geophys Res. https://doi.org/10.1029/2009jf001347
42. Jha SK, Bombardelli FA (2009) Two-phase modeling of turbulence in dilute sediment-laden, open-channel flows. Environ Fluid Mech 9(2):237–266. https://doi.org/10.1007/s10652-008-9118-z
43. Van Deemter JJ, Van der Laan ET (1961) Momentum and Energy balances for dispersed two-phase flow. Appl Sci Res 10:102–108
44. Marble FE (1963) Dynamics of a gas containing small solid particles. Paper presented at the 5th AGRAD symp., Braunschwig, GE
45. Anderson TB, Jackson R (1967) A fluid mechanical description of fluidized bed. Equations of motion. Ind Eng Ind Fundam 6:527–539
46. Tsuo YP, Gidaspow D (1990) Computation of flow patterns in circulating fluidized beds. AIChE J 36(6):885–896
47. Kuipers JAM, Duin KJV, Beckum V, Swaaij WPMV (1992) A numerical model of gas-fluidized beds. Chem Eng Sci 47(8):1913–1924
48. van der Hoef MA, van Sint Annaland M, Deen NG, Kuipers JAM (2008) Numerical simulation of dense gas-solid fluidized beds: a multiscale modeling strategy. Annu Rev Fluid Mech 40(1):47–70. https://doi.org/10.1146/annurev.fluid.40.111406.102130
49. Jenkins JT, Savage SB (1983) A theory for the rapid flow of identical, smooth, nearly elastic, spherical particles. J Fluid Mech. https://doi.org/10.1017/s0022112083001044
50. Lun CKK, Savage SB, Jeffrey DJ, Chepurniy N (1984) Kinetic theories for granular flow: inelastic particles in Couette flow and slightly inelastic particles in a general flowfield. J Fluid Mech 140:223–256. https://doi.org/10.1017/s0022112084000586
51. Ding J, Cidaspow D (1990) A bubbling fluidization model using kinetic theory of granular flow. AIChE J 36(4):523–538
52. Gidaspow D (1994) Multiphase flow and fluidization: continuum and kinetic theory descriptions. Academic, Boston
53. Dickenson JA, Sansalone JJ (2009) Discrete phase model representation of particulate matter (PM) for simulating PM separation by hydrodynamic unit operations. Environ Sci Technol 43(21):8220–8226. https://doi.org/10.1021/es901527r
54. Zahari NM, Zawawi MH, Sidek LM, Mohamad D, Itam Z, Ramli MZ, Syamsir A, Abas A, Rashid M (2018) Introduction of discrete phase model (DPM) in fluid flow: a review. AIP Conf Proc 2030:020234. https://doi.org/10.1063/1.5066875
55. Vakhrushev A, Wu M (2013) Verification of a discrete phase model with water-particle flow experiments in a Tundish. Paper presented at the The 5th international conference STEELSIM, VŠB—Technical University of Ostrava, Czech Republic
56. Marchelli F, Bove D, Moliner C, Bosio B, Arato E (2017) Discrete element method for the prediction of the onset velocity in a spouted bed. Powder Technol 321:119–131. https://doi.org/10.1016/j.powtec.2017.08.032
57. Adamczyk WP, Klimanek A, Białecki RA, Węcel G, Kozołub P, Czakiert T (2014) Comparison of the standard Euler–Euler and hybrid Euler–Lagrange approaches for modeling particle transport in a pilot-scale circulating fluidized bed. Particuology 15:129–137. https://doi.org/10.1016/j.partic.2013.06.008
58. Cloete S, Amini S (2017) Implementing the kinetic theory of granular flows into the lagrangian dense discrete phase model. Paper presented at the 12th international conference on CFD in oil & gas, metallurgical and process industries, SINTEF, Trondheim, Norway
59. Andrews MJ, ORourke PJ (1996) The multiphase particle-in-cell (MP-PIC) method for dense particulate flows. Int J Multiph Flow 22(2):379–402. https://doi.org/10.1016/0301-9322(95)00072-0
60. Snider DM (2001) An incompressible three-dimensional multiphase particle-in-cell model for dense particle flows. J Comput Phys 170(2):523–549. https://doi.org/10.1006/jcph.2001.6747
61. Zeng J, Li H, Zhang D (2019) Numerical simulation of proppant transport in propagating fractures with the multi-phase particle-in-cell method. Fuel 245:316–335. https://doi.org/10.1016/j.fuel.2019.02.056
62. Patankar NA, Joseph DD (2001) Modeling and numerical simulation of particulate flows by the Eulerian-Lagrangian approach. Int J Multiph Flow 27(10):1659–1684. https://doi.org/10.1016/S0301-9322(01)00021-0
63. Cundall PA, Strack ODL (1979) A discrete numerical model for granular assemblies. Geotechnique 29(1):47–65
64. Attard P, Gillies G (2001) Deformation and adhesion of viscoelastic particles: theory and experiment. Aust J Chem 54(8):477–485. https://doi.org/10.1071/Ch01117

65. Gellespie T, Settineri WJ (1968) The effect of capillary liquid on the force of adhesion between spherical solid particles. J Colloid Interface Sci 26:199–202
66. Lian G, Thornton C, Adams MJ (1993) A theoretical study of the liquid bridge forces between two rigid spherical bodies. J Colloid Interface Sci 161:138–147
67. Hamaker HC (1937) The london–van der waals attraction between spherical particlesf. Physica 10:1058–1072
68. Israelachvili JN (2011) Intermolecular and surface forces, 3rd edn. Elsevier Academic Press Inc, San Diego
69. Tsuji Y, Kawaguchi T, Tanaka T (1993) Discrete particle simulation of two-dimensional fluidized bed. Powder Technol 77:79–87
70. Xu BH, Yu AB (1997) Numerical simulation of the gas-solid flow in a fluidized bed by combining discrete particle method with computational fluid dynamics. Chem Eng Sci 52(16):2785–2809
71. Hoomans BPB, Kuipers JAM, Briels WJ, Swaaij WPM (1996) Discrete particle simulation of bubble and slug formation in a two-dimensional gas-fluidised bed: a hard-sphere approach. Chem Eng Sci 51(1):99–118
72. Kawaguchi T, Tanaka T, Tsuji Y (1998) Numerical simulation of two-dimensional fluidized beds using the discrete element method (comparison between the two- and three-dimensional models). Powder Technol 96(2):129–138. https://doi.org/10.1016/S0032-5910(97)03366-4
73. Zhou F, Hu S, Liu Y, Liu C, Xia T (2014) CFD–DEM simulation of the pneumatic conveying of fine particles through a horizontal slit. Particuology 16:196–205. https://doi.org/10.1016/j.partic.2014.03.015
74. Zhou J-w, Du C-l, Liu S-y, Liu Y (2016) Comparison of three types of swirling generators in coarse particle pneumatic conveying using CFD-DEM simulation. Powder Technol 301:1309–1320. https://doi.org/10.1016/j.powtec.2016.07.047
75. Zhang Y, Lim EWC, Wang CH (2007) Pneumatic transport of granular materials in an inclined conveying pipe: comparison of computational fluid dynamics-discrete element method (CFD-DEM), electrical capacitance tomography (ECT), and particle image Velocimetry (PIV) results. Ind Eng Chem Res 46(19):6066–6083. https://doi.org/10.1021/ie061304i
76. Azmir J, Hou Q, Yu A (2019) CFD-DEM simulation of drying of food grains with particle shrinkage. Powder Technol 343:792–802. https://doi.org/10.1016/j.powtec.2018.11.097
77. Hilton JE, Ying DY, Cleary PW (2013) Modelling spray coating using a combined CFD–DEM and spherical harmonic formulation. Chem Eng Sci 99:141–160. https://doi.org/10.1016/j.ces.2013.05.051
78. Suzuki K, Bardet JP, Oda M, Iwashita K, Tsuji Y, Tanaka T, Kawaguchi T (2007) Simulation of upward seepage flow in a single column of spheres using discrete-element method with fluid-particle interaction. J Geotech Geoenviron 133(1):104–109. https://doi.org/10.1061/(Asce)1090-0241(2007)133:1(104)
79. Zou Y, Chen C, Zhang L (2020) Simulating progression of internal erosion in gap-graded sandy gravels using coupled CFD-DEM. Int J Geomech. https://doi.org/10.1061/(asce)gm.1943-5622.0001520
80. Tsuji Y, Tanaka T, Ishida T (1992) Lagrangian numerical-simulation of plug flow of cohesionless particles in a horizontal pipe. Powder Technol 71(3):239–250. https://doi.org/10.1016/0032-5910(92)88030-L
81. Courant R, Friedrichs K, Lewy H (1928) On the partial difference equations of mathematical physics. IBM J Res Dev 11(2):215–234
82. Hirche D, Birkholz F, Hinrichsen O (2019) A hybrid Eulerian–Eulerian–Lagrangian model for gas-solid simulations. Chem Eng J. https://doi.org/10.1016/j.cej.2018.08.129
83. Kloss C, Goniva C, Hager A, Amberger S, Pirker S (2012) Models, algorithms and validation for opensource DEM and CFD-DEM. Progress Comput Fluid Dyn. https://doi.org/10.1504/pcfd.2012.047457
84. Goniva C, Kloss C, Deen NG, Kuipers JAM, Pirker S (2012) Influence of rolling friction on single spout fluidized bed simulation. Particuology 10(5):582–591. https://doi.org/10.1016/j.partic.2012.05.002
85. Pan TW, Joseph DD, Bai R, Glowinski R, Sarin V (2002) Fluidization of 1204 spheres: simulation and experiment. J Fluid Mech 451:169–191. https://doi.org/10.1017/s0022112001006474
86. Hu HH (1996) Direct simulation of flows of solid-liquid mixtures. Int J Multiph Flow 22(2):335–352
87. Catalano E, Chareyre B, Barthelemy E (2014) Pore-scale modeling of fluid-particles interaction and emerging poromechanical effects. Int J Numer Anal Meth Geomech 38(1):51–71. https://doi.org/10.1002/nag.2198
88. Wachs A, Hormozi S, Hrenya C, Pannala S (2018) New frontiers in multiphase CFD for the 21st century energy mix. Workshop final report. https://www.birs.ca/events/2018/5-day-workshops/18w5139. Accessed 12 Aug 2020
89. Cook BK, Noble DR, Williams JR (2004) A direct simulation method for particle-fluid systems. Eng Comput 21(2/3/4):151–168. https://doi.org/10.1108/02644400410519721
90. Kruggel-Emden H, Kravets B, Suryanarayana MK, Jasevicius R (2016) Direct numerical simulation of coupled fluid flow and heat transfer for single particles and particle packings by a LBM-approach. Powder Technol 294:236–251. https://doi.org/10.1016/j.powtec.2016.02.038
91. Cui X, Li J, Chan A, Chapman D (2014) Coupled DEM–LBM simulation of internal fluidisation induced by a leaking pipe. Powder Technol 254:299–306. https://doi.org/10.1016/j.powtec.2014.01.048
92. Hardy J, Depazzis O, Pomeau Y (1976) Molecular-dynamics of a classical lattice gas—transport properties and time correlation-functions. Phys Rev A 13(5):1949–1961. https://doi.org/10.1103/PhysRevA.13.1949
93. Chen S, Doolen GD (1998) Lattice Boltzmann method for fluid flows. Annu Rev Fluid Mech 30:329–364. https://doi.org/10.1146/annurev.fluid.30.1.329
94. Qian YH, Dhumieres D, Lallemand P (1992) Lattice Bgk models for Navier-Stokes equation. Europhys Lett 17(6):479–484. https://doi.org/10.1209/0295-5075/17/6/001
95. Satofuka N, Nishioka T (1999) Parallelization of lattice Boltzmann method for incompressible flow computations. Comput Mech 23(2):164–171. https://doi.org/10.1007/s004660050397
96. Third JR, Chen Y, Müller CR (2015) Comparison between finite volume and lattice-Boltzmann method simulations of gas-fluidised beds: bed expansion and particle–fluid interaction force. Comput Particle Mech 3(3):373–381. https://doi.org/10.1007/s40571-015-0086-z
97. Han Y, Cundall P (2017) Verification of two-dimensional LBM-DEM coupling approach and its application in modeling episodic sand production in borehole. Petroleum 3(2):179–189. https://doi.org/10.1016/j.petlm.2016.07.001
98. Tang Y, Chan DH, Zhu DZ (2017) A coupled discrete element model for the simulation of soil and water flow through an orifice. Int J Numer Anal Meth Geomech 41(14):1477–1493. https://doi.org/10.1002/nag.2677
99. Tang Y, Chan DH, Zhu DZ (2017) Numerical investigation of sand-bed erosion by an upward water Jet. J Eng Mech. https://doi.org/10.1061/(asce)em.1943-7889.0001319
100. Lucy LB (1977) Numerical approach to testing of fission hypothesis. Astron J 82(12):1013–1024. https://doi.org/10.1086/112164

101. Gingold RA, Monaghan JJ (1977) Smoothed particle hydrodynamics—theory and application to non-spherical stars. Mon Not R Astron Soc 181(2):375–389. https://doi.org/10.1093/mnras/181.3.375
102. Koshizuka S, Oka Y (1996) Moving-particle semi-implicit method for fragmentation of incompressible fluid. Nucl Sci Eng 123(3):421–434. https://doi.org/10.13182/nse96-a24205
103. Sulsky D, Zhou SJ, Schreyer HL (1995) Application of a particle-in-cell method to solid mechanics. Comput Phys Commun 87(1–2):236–252. https://doi.org/10.1016/0010-4655(94)00170-7
104. Sulsky D, Brackbill JU (1991) A numerical-method for suspension flow. J Comput Phys 96(2):339–368. https://doi.org/10.1016/0021-9991(91)90240-L
105. Bui HH, Fukagawa R (2013) An improved SPH method for saturated soils and its application to investigate the mechanisms of embankment failure: case of hydrostatic pore-water pressure. Int J Numer Anal Meth Geomech 37(1):31–50. https://doi.org/10.1002/nag.1084
106. Cleary PW, Monaghan JJ (1999) Conduction modelling using smoothed particle hydrodynamics. J Comput Phys 148(1):227–264. https://doi.org/10.1006/jcph.1998.6118
107. Gotoh H, Okayasu A, Watanabe Y (2013) Computational wave dynamics. Advanced series on ocean engineering, vol 37. World Scientific, Hackensack
108. Shao SD, Lo EYM (2003) Incompressible SPH method for simulating Newtonian and non-Newtonian flows with a free surface. Adv Water Resour 26(7):787–800. https://doi.org/10.1016/S0309-1708(03)00030-7
109. Khayyer A, Gotoh H (2010) A higher order Laplacian model for enhancement and stabilization of pressure calculation by the MPS method. Appl Ocean Res 32(1):124–131. https://doi.org/10.1016/j.apor.2010.01.001
110. Khayyer A, Gotoh H (2009) Wave impact pressure calculations by improved SPH methods. Int J Offshore Polar 19(4):300–307
111. Khayyer A, Gotoh H, Shimizu Y (2017) Comparative study on accuracy and conservation properties of two particle regularization schemes and proposal of an optimized particle shifting scheme in ISPH context. J Comput Phys 332:236–256. https://doi.org/10.1016/j.jcp.2016.12.005
112. Khayyer A, Gotoh H, Shao S (2009) Enhanced predictions of wave impact pressure by improved incompressible SPH methods. Appl Ocean Res 31(2):111–131. https://doi.org/10.1016/j.apor.2009.06.003
113. Wang Z, Zhang J, Shirazi SA, Dou Y (2019) Experimental and numerical study of erosion in a non-Newtonian hydraulic fracturing fluid. Wear 422–423:1–8. https://doi.org/10.1016/j.wear.2018.12.080
114. Khayyer A, Gotoh H, Falahaty H, Shimizu Y (2018) An enhanced ISPH–SPH coupled method for simulation of incompressible fluid–elastic structure interactions. Comput Phys Commun 232:139–164. https://doi.org/10.1016/j.cpc.2018.05.012
115. Marrone S, Antuono M, Colagrossi A, Colicchio G, Le Touzé D, Graziani G (2011) δ-SPH model for simulating violent impact flows. Comput Methods Appl Mech Eng 200(13–16):1526–1542. https://doi.org/10.1016/j.cma.2010.12.016
116. Potapov AV, Hunt ML, Campbell CS (2001) Liquid–solid flows using smoothed particle hydrodynamics and the discrete element method. Powder Technol 116:204–213
117. Sakai H, Maeda K (2006) Seepage failure of granular ground accounting for soil-water-gas interaction. In: Geomechanics and geotechnics of particulate media, proceedings of the international symposium on geomechanics and geotechnics of particulate media, Ube, Yamaguchi, Japan, pp 273–279
118. Biot MA (1941) General theory of three-dimensional consolidation. J Appl Phys 12(2):155–164. https://doi.org/10.1063/1.1712886
119. Robinson M, Ramaioli M, Luding S (2014) Fluid–particle flow simulations using two-way-coupled mesoscale SPH–DEM and validation. Int J Multiph Flow 59:121–134. https://doi.org/10.1016/j.ijmultiphaseflow.2013.11.003
120. Kwon J, Cho H (2016) Simulation of solid-liquid flows using a two-way coupled smoothed particle hydrodynamics-discrete element method model. Korean J Chem Eng 33(10):2830–2841. https://doi.org/10.1007/s11814-016-0193-4
121. Wu K, Yang D, Wright N (2016) A coupled SPH–DEM model for fluid-structure interaction problems with free-surface flow and structural failure. Comput Struct 177:141–161. https://doi.org/10.1016/j.compstruc.2016.08.012
122. Tang Y, Jiang Q, Zhou C (2018) A Lagrangian-based SPH–DEM model for fluid–solid interaction with free surface flow in two dimensions. Appl Math Model 62:436–460. https://doi.org/10.1016/j.apm.2018.06.013
123. He Y, Bayly AE, Hassanpour A, Muller F, Wu K, Yang D (2018) A GPU-based coupled SPH–DEM method for particle-fluid flow with free surfaces. Powder Technol 338:548–562. https://doi.org/10.1016/j.powtec.2018.07.043
124. Xu W-J, Dong X-Y, Ding W-T (2019) Analysis of fluid-particle interaction in granular materials using coupled SPH–DEM method. Powder Technol 353:459–472. https://doi.org/10.1016/j.powtec.2019.05.052
125. Gholami Korzani M, Galindo-Torres SA, Scheuermann A, Williams DJ (2017) SPH approach for simulating hydro-mechanical processes with large deformations and variable permeabilities. Acta Geotech. https://doi.org/10.1007/s11440-017-0610-9
126. Wang C, Wang Y, Peng C, Meng X (2016) Smoothed particle hydrodynamics simulation of water-soil mixture flows. J Hydraul Eng. https://doi.org/10.1061/(asce)hy.1943-7900.0001163
127. Khayyer A, Gotoh H, Shimizu Y, Gotoh K, Falahaty H, Shao S (2018) Development of a projection-based SPH method for numerical wave flume with porous media of variable porosity. Coast Eng 140:1–22. https://doi.org/10.1016/j.coastaleng.2018.05.003
128. Akbari H, Pooyarad A (2020) Wave force on protected submarine pipelines over porous and impermeable beds using SPH numerical model. Appl Ocean Res. https://doi.org/10.1016/j.apor.2020.102118
129. Naili M, Matsushima T, Yamada Y (2005) A 2D smoothed particle hydrodynamics method for liquefaction induced lateral spreading analysis. J Appl Mech 8:591–599. https://doi.org/10.2208/journalam.8.591
130. Zhang W, Maeda K, Saito H, Li Z, Huang Y (2016) Numerical analysis on seepage failures of dike due to water level-up and rainfall using a water–soil-coupled smoothed particle hydrodynamics model. Acta Geotech 11(6):1401–1418. https://doi.org/10.1007/s11440-016-0488-y
131. Huang Y, Zhang W, Mao W, Jin C (2011) Flow analysis of liquefied soils based on smoothed particle hydrodynamics. Nat Hazards 59(3):1547–1560. https://doi.org/10.1007/s11069-011-9851-3
132. Ariyaratne WKH, Manjula EVPJ, Ratnayake C, Melaaen MC (2016) CFD Approaches for modeling gas-solids multiphase flows—a review. Paper presented at the Proceedings of The 9th EUROSIM congress on modelling and simulation, EUROSIM 2016, The 57th SIMS conference on simulation and modelling SIMS 2016
133. Zhou H, Wang G, Jia C, Li C (2019) A Novel, coupled CFD-DEM model for the flow characteristics of particles inside a pipe. Water. https://doi.org/10.3390/w11112381

134. Norouzi HR, Zarghami R, Sotudeh-Gharebagh R, Mostoufi N (2016) Coupled CFD-DEM modeling: formulation, implementation, and application to multiphase flows, 1st edn. Wiley, Oxford
135. Konrad K, Davidson JF (1984) The gas-liquid analogy in horizontal dense-phase pneumatic conveying. Powder Technol 39(2):191–198. https://doi.org/10.1016/0032-5910(84)85036-6
136. Link JM, Deen NG, Kuipers JAM, Fan X, Ingram A, Parker DJ, Wood J, Seville JPK (2008) PEPT and discrete particle simulation study of spout-fluid bed regimes. AIChE J 54(5):1189–1202. https://doi.org/10.1002/aic.11456
137. MFiX MFiX hybrid Eulerian–Lagrangian–Eulerian. https://mfix.netl.doe.gov/doc/mfix/19.1.4/about.html
138. Zhao T, Dai F, Xu NW (2017) Coupled DEM-CFD investigation on the formation of landslide dams in narrow rivers. Landslides 14(1):189–201. https://doi.org/10.1007/s10346-015-0675-1
139. Khayyer A, Tsuruta N, Shimizu Y, Gotoh H (2019) Multi-resolution MPS for incompressible fluid-elastic structure interactions in ocean engineering. Appl Ocean Res 82:397–414. https://doi.org/10.1016/j.apor.2018.10.020
140. Auton TR, Hunt JCR, Prudhomme M (1988) The force exerted on a body in inviscid unsteady non-uniform rotational flow. J Fluid Mech 197:241–257. https://doi.org/10.1017/S0022112088003246
141. Reeks MW, Mckee S (1984) The dispersive effects of basset history forces on particle motion in a turbulent-flow. Phys Fluids 27(7):1573–1582. https://doi.org/10.1063/1.864812
142. Saffman PG (1968) Correction. J Fluid Mech 31:624. https://doi.org/10.1017/S0022112068999990
143. Saffman PG (1965) Lift on a small sphere in a slow shear flow. J Fluid Mech 22:385. https://doi.org/10.1017/S0022112065000824
144. Rubinow SI, Keller JB (1961) The transverse force on a spinning sphere moving in a viscous fluid. J Fluid Mech 11(3):447–459. https://doi.org/10.1017/s0022112061000640
145. Sakai M, Shigeto Y, Sun X, Aoki T, Saito T, Xiong J, Koshizuka S (2012) Lagrangian-Lagrangian modeling for a solid–liquid flow in a cylindrical tank. Chem Eng J 200–202:663–672. https://doi.org/10.1016/j.cej.2012.06.080
146. Idelsohn SR, Oñate E, Pin FD (2004) The particle finite element method: a powerful tool to solve incompressible flows with free-surfaces and breaking waves. Int J Numer Meth Eng 61(7):964–989. https://doi.org/10.1002/nme.1096
147. Fullmer WD, Hrenya CM (2018) Continuum prediction of scale-dependent, anisotropic fluctuating kinetic energy in gas-solid flows. Chem Eng Sci 186:84–87. https://doi.org/10.1016/j.ces.2018.04.035
148. Passalacqua A, Fox RO (2011) Implementation of an iterative solution procedure for multi-fluid gas–particle flow models on unstructured grids. Powder Technol 213(1–3):174–187. https://doi.org/10.1016/j.powtec.2011.07.030
149. Sousani M, Hobbs AM, Anderson A, Wood R (2019) Accelerated heat transfer simulations using coupled DEM and CFD. Powder Technol 357:367–376. https://doi.org/10.1016/j.powtec.2019.08.095
150. Bakshi A, Shahnam M, Gel A, Li T, Altantzis C, Rogers W, Ghoniem AF (2018) Comprehensive multivariate sensitivity analysis of CFD-DEM simulations: critical model parameters and their impact on fluidization hydrodynamics. Powder Technol 338:519–537. https://doi.org/10.1016/j.powtec.2018.06.049
151. Fernandes C, Semyonov D, Ferrás LL, Nóbrega JM (2018) Validation of the CFD-DPM solver DPMFoam in OpenFOAM® through analytical, numerical and experimental comparisons. Granul Matter. https://doi.org/10.1007/s10035-018-0834-x
152. Chen F, Drumm EC, Guiochon G (2011) Coupled discrete element and finite volume solution of two classical soil mechanics problems. Comput Geotech 38(5):638–647. https://doi.org/10.1016/j.compgeo.2011.03.009
153. Peng C, Wang S, Wu W, Yu H-s, Wang C, Chen J-y (2019) LOQUAT: an open-source GPU-accelerated SPH solver for geotechnical modeling. Acta Geotech 14(5):1269–1287. https://doi.org/10.1007/s11440-019-00839-1

Publisher's Note Springer Nature remains neutral with regard to jurisdictional claims in published maps and institutional affiliations.